Nanoscale Advances

ROYAL SOCIETY OF CHEMISTRY

REVIEW

View Article Online
View Journal | View Issue

Cite this: *Nanoscale Adv.*, 2024, **6**, 2539

Bioinspired graphene-based metal oxide nanocomposites for photocatalytic and electrochemical performances: an updated review

Ajay K. Potbhare,[a] S. K. Tarik Aziz,[b] Mohd. Monis Ayyub,[c] Aniket Kahate,[a] Rohit Madankar,[a] Sneha Wankar,[d] Arnab Dutta,[b] Ahmed Abdala,[e] Sami H. Mohmood,*[f] Rameshwar Adhikari*[g] and Ratiram G. Chaudhary*[a]

Considering the rapidly increasing population, the development of new resources, skills, and devices that can provide safe potable water and clean energy remains one of the vital research topics for the scientific community. Owing to this, scientific community discovered such material for tackle this issue of environment benign, the new materials with graphene functionalized derivatives show significant advantages for application in multifunctional catalysis and energy storage systems. Herein, we highlight the recent methods reported for the preparation of graphene-based materials by focusing on the following aspects: (i) transformation of graphite/graphite oxide into graphene/graphene oxide *via* exfoliation and reduction; (ii) bioinspired fabrication or modification of graphene with various metal oxides and its applications in photocatalysis and storage systems. The kinetics of photocatalysis and the effects of different parameters (such as photocatalyst dose and charge-carrier scavengers) for the optimization of the degradation efficiency of organic dyes, phenol compounds, antibiotics, and pharmaceutical drugs are discussed. Further, we present a brief introduction on different graphene-based metal oxides and a systematic survey of the recently published research literature on electrode materials for lithium-ion batteries (LIBs), supercapacitors, and fuel cells. Subsequently, the power density, stability, pseudocapacitance charge/discharge process, capacity and electrochemical reaction mechanisms of intercalation, and conversion- and alloying-type anode materials are summarized in detail. Furthermore, we thoroughly distinguish the intrinsic differences among underpotential deposition,

Received 1st December 2023
Accepted 4th April 2024

DOI: 10.1039/d3na01071f

rsc.li/nanoscale-advances

[a]*Post Graduate Department of Chemistry, Seth Kesarimal Porwal College of Arts and Science and Commerce, Kamptee-441001, India. E-mail: chaudhary_rati@yahoo.com*
[b]*Chemistry Department, Indian Institute of Technology, Bombay, Powai 400076, India*
[c]*New Chemistry Unit, International Centre for Materials Science and Sheikh Saqr Laboratory, Jawaharlal Nehru Centre for Advanced Scientific Research, Bangalore, India*
[d]*Post Graduate Teaching Department of Chemistry, Gondwana University, Gadchiroli 442605, India*
[e]*Chemical Engineering Program, Texas A&M University at Qatar POB, 23784, Doha, Qatar*
[f]*Department of Physics, The University of Jordan, Amman 11942, Jordan. E-mail: s.mahmood@ju.edu.jo*
[g]*Central Department of Chemistry and Research Centre for Applied Science and Technology (RECAST), Tribhuvan University, Kathmandu, Nepal. E-mail: nepalpolymer@yahoo.com*

Ratiram G. Chaudhary

Dr Ratiram Gomaji Chaudhary is presently working as Associate Professor and Head in the Post-Graduate Department of Chemistry, Seth Kesarimal Porwal College, Kamptee. He is a Senate member of RTM Nagpur University, Nagpur. He is a BoS member of Chemistry, and also worked as a Task Force member and on several committees of R. T. M. N. U., Nagpur. Recently, he received the 'Best Researcher Award-2023' by R. T. M. N. U. Nagpur, and also Shikshan Prasarak Mandal, Kamptee. His research areas of interest are biogenic synthesis, graphene-based nanohybrids, photocatalysis, and microbial assays. He has completed one MRP funded by SERB/DST. He is a recognized supervisor and produced six PhD students, while seven are still working, and completed 65 MSc projects. Moreover, he is a recipient of the JRF award from UGC and many more awards. He has published 6 books, 26 book chapters, and 146 articles in SCI/Scopus indexing journals, having a citation of 2296 with an h*-index of 27. He is a reviewer of 68 SCI/Scopus journals. He worked as Guest Editor for four thematic issue which was published by Elsevier and Bentham Science publishers. Moreover, he has delivered several Invited/Resource talks, and deputed as a Chairpersons in various international conferences which was held in Sweden, Finland, Nepal, Argentina, Delhi, Allahabad, Kottayam, Kerala, Nagpur* etc.

intercalation, and conventional pseudocapacitance of electrode materials. This review offers a meaningful reference for the construction and fabrication of graphene-based metal oxides as effective photocatalysts for photodegradation study and high-performance optimization of anode materials for LIBs, supercapacitors, and fuel cells.

1. Introduction

Green nanotechnology is a laudable approach in the area of science and technology owing to the demand for cheaper, rapid, and non-hazardous biochemicals and their incredible properties. However, conventional techniques are being widely employed for the fabrication of nanomaterials (NMs) such as metals, metal oxides, quantum dots, carbon nanotubes (CNTs), and carbon-based NMs. Thus, the development of new manufacturing methods and evaluation of the atomic, molecular and macromolecular scales to create new materials with extraordinary trademarks that have excellent electrical, optical, magnetic, and catalytic properties are necessary.[1,2] One of the extraordinary advanced materials discovered in the past two decades in the field of nanoscience and nanotechnology is graphene-based materials. Graphene is a promising and exciting material of the 21st century. It is densely packed in a honeycomb lattice with thin layers of sp^2 hybridized carbon atoms (Fig. 1). Graphene composed of accurately arranged two-dimensional (2D) sheets displaying high crystallites with unique electronic qualities, thus emerging as an encouraging new NMs for a variety of stimulating applications despite of its short history. A. Geim and K. Novoselov (2004) were pioneers of this "miracle material", which has attracted vast interest among scientists, resulting in an inundation of studies dedicated to the various features of graphene in the last few years.[3] Recently, this (2D) single sheet of carbon dervatives of graphene has been proven to be highly well-organized for a wide range of applications, which is mainly attributed to its large surface area (2600 $m^2\ g^{-1}$), high Young's modulus (1.0 TPa), and extraordinary thermal conductivity (~5000 W $m^{-1}\ K^{-1}$).[4,5] It also displays single-molecule gas detection sensitivity,[6] quantum captivity in nanoscale ribbons,[7] extensive range of ballistic transport at RT[8] and high optical transmittance (~97.7%).[9]

These exclusive properties of graphene have revealed its extensive range of applications in various branches of nanotechnology (Fig. 2), for example, anti-bacterial activity,[10] *in vitro* toxicity to various cell lines, DNA degradation, photocatalytic activity, lithium-ion batteries,[11–14] fuel cells, catalyst engineering,[15,16] chemically derived sensors,[17] biosensors,[18] antimicrobial activity,[19] flexible thin-film transistors,[20] biomedical applications, drugs delivery,[21,22] solar cells,[23] photovoltaic devices,[24] imaging,[25] P–N junction diodes,[26] graphene-based super capacitors,[27] solar panels,[28] electromagnetic shielding,[29] water purification,[30] absorption of non-aqueous liquids, *e.g.*, oils, aromatic compounds, alkenes, dyes, and organic compounds, removal of organic pollutants and pharmaceutical drugs, and remediation of pesticides and heavy metal ionic solutions.[31–35] In this case, large quantities of graphene materials are necessary to satisfy the vast demands of the above-mentioned applications.

However, the fabrication of high-quality graphene *via* an economical route and its large-scale production are significant challenges. To date, numerous methodologies have been developed to fabricate graphene from pristine graphite, for instance epitaxial growth,[36] vacuum-based thermal annealing,[37] non-catalytic synthesis,[38] Scotch tape method,[39] micromechanical cleavage,[40] (CVD),[41] thermal exfoliation,[42] CNT cutting,[43] liquid-phase exfoliation,[44] ultrasonication,[45] and reduction of graphene oxide.[46] There are also other alternative and harmful methods for the production of graphene oxide including chemical discharge,[47] discharging arc[48] and CNT unzipping.[49] Epitaxial growth is capable of producing great-quality multilayer graphene but cannot separate single conductive layers/bilayers that are excellent for energy storage applications.[50] A significant constraint of micromechanical cleavage is repetitive cycles of detaching throughout the layer exclusion and it is very difficult to maintain the number of isolated layers fabricated by this technique.[51]

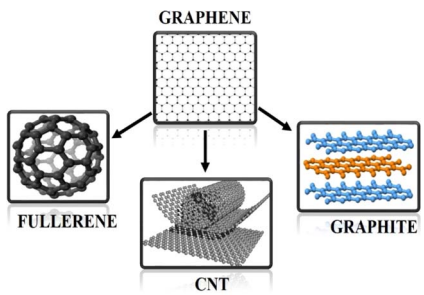

Fig. 1 Graphene is a 2D building block for carbonaceous materials of all other dimensions. It can be wrapped into 0D buckyballs, rolled into 1D nanotubes or stacked into 3D graphite.

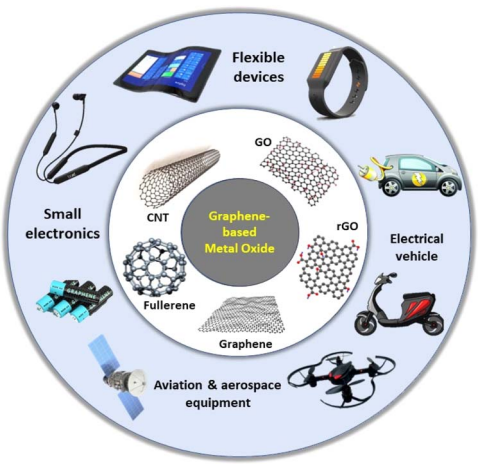

Fig. 2 Overview of graphene-based materials for advanced energy storage devices and their potential applications in various fields.

Alternatively, thermal exfoliation requires high manufacturing prices.[40] Meanwhile, in CVD, it is difficult to accomplish layer separation without the destruction of the material and effective exfoliation from the substrate is uncertain. In contrast, the reduction of graphene oxide (GO) is considered an encouraging methodology for the mass fabrication of graphene. The product achieved by this technique is usually designated as reduced graphene oxide (rGO) or nanostructure graphene (NSG).[52] As an alternative method, the liquid-phase exfoliation technique, which involves the process of ultrasonication[53] or mixing[54] of a stabilizer containing graphite to preclude the accumulation of graphene to graphite, is also commonly employed by researchers due to its easy synthesis of graphene and wide flexibility in terms of the selected mixing device. Furthermore, the final product is a graphene solution after a centrifugation phase, and the application of liquid-exfoliated graphene can be additionally introduced into graphene paper by vacuum percolation,[55] conductive ink[56] or nanofluids.[57]

Alternatively, rGO/NSG can be synthesized from graphene oxide *via* green methods. Firstly, GO is fabricated from graphite powder through oxidative reaction, which comprehensively enriches the sheets with altered oxygen groups. The presence of abundant oxygen moieties functionalized on the basal plane of carbon makes GO electrically insulating, and also induces thermal instability.[58] Therefore, the molecules of oxygen are reduced and significantly relocated to the π-lattice. This is beneficial to produce thermally established graphene and recapture electronic conductivity. Some GO reduction methods, *e.g.*, electrochemical,[59,60] thermal,[61] photocatalytic,[62] and chemical methods, have been described recently. Among them, electrochemical reduction is incompetent to heal the inherent deficiencies in the GO precursor. Also, in the case of the exfoliation of GO to single-layer sheets requires a lower content of oxygen in the GO precursor. Given that a low content of oxygen reduces the interaction within the oxygen functionalities of GO, stable species can be produced such as in-plane ether or out-of-plane carbonyl groups, which are reasonably tough to eliminate by the electrochemical reduction method.[63] Presently, deoxygenation by the thermal method is economical. It is a complex phenomenon due to the thermal-energy prompted multi-step elimination process of introduced H_2O and other oxide groups of –OH, –COOH and epoxy groups.[64] Photocatalytic reduction involves dynamic activity of light-sensitive materials under UV emission.[65] Hence, in contrast with the above-mentioned reduction methods, chemical reduction is considered the easiest technique to yield ultrathin graphene sheets with great crosswise dimensions and area.[66] Furthermore, this technique is practically fast, inexpensive, facile, and appropriate for repeated handling and chemical variations.

Researchers have employing various types of reducing agents to transform GO to graphene *via* the reduction process. However, hydrazine, $LiAlH_4$, $NaBH_4$, hydroquinone, NaOH, *etc.* are noxious in nature, which are unfortunately harmful to the ecosystem. In particular, hydrazine has some drawbacks, for example, during the elimination of the oxygen functional groups, nitrogen tends to covalently interact with GO, forming hydrazones, amines, aziridines, *etc.* These C–N residuals are effective as n-type dopants and have a significant impact on the electronic structure of chemically derived rGO.[67] These sheets have higher resistance, hindering their application. However, there are no simple techniques to remove these impurities, which may be present in a C : N ratio of 16.1 : 1, as reported by Stankovich *et al.* Therefore, as an alternative method, researchers have focused on the use of different types of biochemical constituents, amino acids, plant extract, bacteria, yeast, fungus cells, polysaccharides compounds and metal powders to prepare reduced graphene sheets from GO. These reducing agents are termed "green reducers", given that they are free from carcinogenicity, corrosion, and toxicity. However, review articles are available on chemical or other reduction of GO,[68,69] especially an overview of the green reduction of GO to graphene. Therefore, in this review, we summarize the reduction of GO using different environmentally friendly reducing agents reported recently.

Presently, graphene/inorganic NP-based nanocomposites have attracted significant interest as an advanced era of nanohybrid materials.[70,71] The interest in the scientific community in these materials is continuously increasing due to their individualities in combining the desirable properties of building blocks for application.[72] The innovative magnetic, catalytic, and optoelectronic properties of graphene NCs based on hybridization with NPs have been exploited in various applications, including antibacterial coating, catalysis, sensors, detectors, electronics, imaging, and energy storage (Fig. 3).[73–78]

To date, metals, metal oxides and graphene have been combined to form unique nanomaterials with various properties due to the synergistic effect among these materials, which enhances their properties.[79] These combinations of metal oxide NPs on graphene sheets restrict their re-stacking and agglomeration, thus improving the surface area of the prepared NMs. In addition to enhancing the properties of graphene, the NPs also act as stabilizers against the agglomeration of individual graphene sheets, which is caused by the strong van der Waals interactions between the graphene layers.[80] Moreover, in several cases, the insertion of metallic NPs in graphene also simplifies

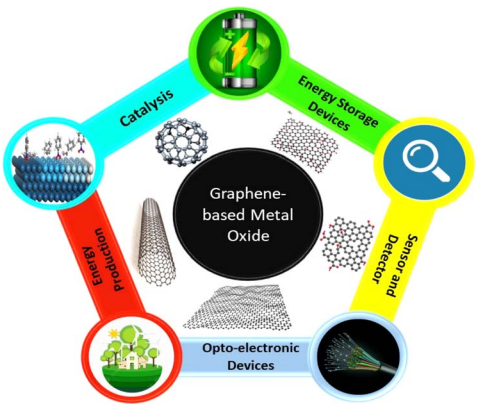

Fig. 3 Schematic diagram of graphene-based metal oxides and their electrochemical applications.

the exfoliation of specific graphene layers from graphite. Thus, more efforts and development of new approaches to synthesize graphene-based nanocomposites (NCs) are indispensable. The decoration of metallic NPs on graphene sheets for the fabrication of graphene-based NCs can be achieved *via* two different methods, as follows:[81] (i) post immobilization (*ex situ* hybridization) and (ii) *in situ* binding (*in situ* crystallization). *Ex situ* hybridization involves the mixing of separate graphene nanosheet solutions and pre-synthesized or commercially available NPs.[82] Alternatively, *in situ* binding of NPs is carried out through the simultaneous reduction of respective metallic salts and graphene oxide (GO) with various reductants.[83] Generally, NPs prepared *via in situ* binding methods have been broadly used due to their cost-effectiveness given that they reduce the number of steps to obtain the desired product.[84] Several reduction techniques have been applied during the *in situ* preparation of graphene NCs, *e.g.* chemical, thermal, bio-inspired, or green and electrochemical reduction. Among them, chemical reduction is the most promising and widely applied method for the large-scale production of graphene metallic NP-based NCs,[85–87] but this method has several disadvantages due to the use of toxic chemicals in synthesis process. Therefore, recently, the trend of applying green reductants in the synthesis of NMs has gained popularity.[88] For example, a variety of green reductants has been applied for the synthesis of metallic NPs, such as plant extracts, vitamin C, amino acids, ascorbic acid, glucose, bovine serum albumin and microorganisms (bacteria, fungi, and yeast).[89–92] Among them, plant extracts have received remarkable interest due to their cost effectiveness, eco-friendly nature, easy availability and bulk quantities.[93] Additionally, plant extracts not only act as green reducing agents but also function as capping and stabilizing agents, which limit the use of additional chemical stabilizers.[94] Consequently, plant extracts have not only been employed to reduce metallic NPs, but in many cases, they have also been effectively applied for the reduction of GO.[95] However, although a series of metallic NPs has been synthesis using plant extracts as a green reducing agents, their application in the synthesis of graphene-based NCs has been limited thus far.[96–98]

The enhancement of these advanced composite materials has facilitated their application in energy storage systems including Li-ion batteries, fuel cells and supercapacitors, or even energy systems such as photovoltaic devices and photocatalysis. These scopes were well-addressed in the review articles by Huang *et al.*[99] and Chen *et al.*,[100] respectively, from the standpoint of electrochemistry. They significantly discussed the up-to-date synthesis techniques, together with the electron transfer properties, involving the electronic structure and electron transport in the graphene composite NSs.

Presently, although the incredible developments in science and technology have certainly improved the quality and standard of human life and health, they have created a multitude of problems as well. Among them, water pollution and contamination are one of the biggest and the most alarming problems that demands formidable and effective solutions. Predominantly, in developing countries, the situation is worrisome, and the non-availability of inexpensive water treatment systems further aggravates the situation.[101] Although huge initiatives are already underway to tackle this problem, further and highly rigorous research dedicated to this issue is still required. In recent times, graphene-functionalized semiconductor (metal oxide) photocatalysts have captivated significant attention towards the scientific community due to their large surface area, tunable band gap, good electron conductivity, and high capacity of light adsorption.[102,103] The primary demonstration by Fujishima and Honda in 1972 of the electrochemical splitting of water on TiO_2 electrodes using photons[104] was a significant development. Since then, graphene-based metal oxide semiconductor photocatalysts have been employed in solar energy conversion, degradation of various water pollutants and environmental remediation, as shown in Fig. 4. Some semiconductor photocatalysts including TiO_2, CuO, BiOCl, ZnO, CdO, CdS, $ZnWO_4$, SnO_2, $NiFe_2O_4$, Bi_2O_3/BiOCl, and $MnFe_2O_4$ can act as light-induced photocatalysts for the degradation of pollutants.

Abd Elkodous *et al.*[105] synthesized a $Co_{0.5}Ni_{0.5}Fe_2O_4/SiO_2/TiO_2$ layer-by-layer matrix loaded with C-dots, rGO and SWCNTs, acting as an electron reservoir for photocatalytic degradation. The photocatalytic properties of the fabricated nanocomposites were compared with the standard TiO_2 (P_{25}). The kinetics of the photocatalysis and the role of charge scavengers were studied in detail.

Ecological energy creation, economically sustainable expansion, and reasonable healthcare are three key challenges of the present global society. Electrochemistry is the basis of many chemicals, and also biological sensors, energy storage devices and new-generation tools. Electrochemistry consumes energy in the sparkling form as electricity to assemble or introduce electrons through electrodes. New innovative materials are always pursued for existing devices to improve their performances or generate new technologies. Graphene and associated materials induce innovative perceptions and projections in electrochemical systems. The electrochemical devices established by graphene exhibit certain advantages. One of the objectives of this review is to offer a critical outline on the electrochemistry of graphene-based metal oxide NCs and related materials. Subsequently, we focus on numerous applications of graphene-based metal oxide NCs in electrochemical devices, including supercapacitors, fuel cells, rechargeable ion batteries, sensors and biosensors and the release of electrical energy *via*

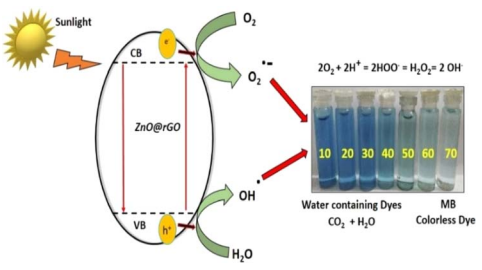

Fig. 4 Electron transfer from the conduction band of MO to graphene through the percolation mechanism of dye degradation. Reproduced with permission from Elsevier. Copyright 2021.

electrochemical practices in an efficient, reversible, and expedient way, which have been extensively used in several fields such as moveable electronics, electrical vehicles (EVs), and aviation/aerospace tools including sensors and biosensors, and then energy storage and new-generation applications.[106] We critically discuss the advantages and drawbacks of graphene-based NCs and outline their future challenges.

The selective illustration of electrode materials as NS materials has presented the opportunity to design novel energy-storage materials for next-generation devices such as high-performance LIBs, supercapacitors and fuel cells, which have played a prominent role among the sustainable energy technologies, and in particular have attracted significant research interest in the past few years owing to their elevated higher power density, higher energy density, and longer cycle life. Due to the high surface area and specific configuration of NS materials, these electrodes can provide high lithium-ion flux across the interface, short diffusion pathways for both Li ions and electrons, abundant active sites for Li storage, high freedom for volume changes during the electrochemical charge/discharge process, and long cycle stability with superior specific capacitance.[107]

Over the years, various types of materials, such as carbon-based NCs, have become readily accessible for electrochemical application. Especially, graphene-based metal oxides/hydroxides, mixed metal oxides, layered double hydroxides, carbonaceous materials, conducting polymers, inorganic carbides, nitrides, *etc.* have been extensively considered as electrodes materials. Graphene-based metal oxide electrodes are cost effective and have high permeability, allowing the simple penetration of electrolytes into electrodes and improving the capacitance. Besides, their large surface area, operative electrical conductivity and rich redox activity make them suitable for electric SCs with double-layer capacitance (electric double-layer capacitance).[108,109]

Similarly, Kumar *et al.*[110] synthesized cost-effective novel N-rGO@CoO NCs *via* the microwave technique. In this work, CoO nanocrystals were decorated on 2D N-doped rGO nanosheets (NSs) as an excellent electrode material, which showed superior cyclic stability and specific capacitance. The optimized N-rGO@CoO electrodes exhibited a specific capacitance value of 744.1 F g^{-1}. Also, the stability of NCs was demonstrated, with the electrode retaining about 91.3% of its original specific capacitance even after 5000 cycles. Also, Youssry *et al.* synthesized TrGO/Ni NCs using the thermal method using nickel foam (NF) as a substrate under the inert atmosphere of nitrogen gas.[111] The as-synthesized TrGO/Ni electrode achieved a very high specific capacitance of 617 f g^{-1} at a scan rate of 2 mV s^{-1}. The TrGO/Ni NCs exhibited long-term stability over 2000 cycles at a scan rate of 50 mV s^{-1} with a capacitance retention of 90.2%.

Kumar *et al.* studied the simple and cost-effective microwave synthesis of rGO NSs combined with iron oxide for supercapacitor electrodes. In the resulting rGO@Fe_3O_4 composites, the faceted-Fe_3O_4 NPs were homogeneously distributed on the surfaces of the rGO NSs. The material revealed a maximum value of specific capacitance (771.3 F g^{-1} at 5 mV s^{-1}), with outstanding cyclic stability (95.1% after 5000 cycles). The results indicated that the homogeneous microwave-processed material is a promising candidate for SC applications.[112]

Also, Kumar *et al.*[113] achieved highly dispersed TiO_2 nanoparticles (NPs) on graphene NSs *via* hydrothermal treatment. The hybrid graphene TiO_2 NS composite (H-GTN) showed enhanced optical and electrochemical properties for future application as a supercapacitor. The cyclic voltammetry test for H-GTN showed a very high specific capacitance value of up to 530 F g^{-1} at a scan rate of 3 mV s^{-1}, and nearly stable capacitance of 400 F g^{-1} above 20 mV s^{-1}, showing long cyclic stability. Similarly, Youssry *et al.*[114] demonstrated a feasible way to fabricate Co–Ni LDH NS electrode materials on Ni foam *via* the electrochemical deposition method. The electrochemical deposition of Co–Ni LDH NSs was achieved by cyclic voltammetry. The Co–Ni LDH NS electrode materials synthesized at 8 cycles exhibited an enhanced electrochemical efficiency and provided a superior capacitance of 3130.8 F g^{-1}. Furthermore, Co–Ni LDH NSs was stable over 3000 cycles with a capacitance retention of 72.4%.

Kumar *et al.*[115] carried out a one-step rapid and facile microwave-assisted synthesis process for fabricating ZnOL@MpEG hybrids and investigated their application as electrode materials. In this synthesis process, the microwave-assisted deposition of ZnO layers occurred on microwave partially exfoliated graphene (MpEG) sheets to obtain the ZnOL@MpEG hybrids, which demonstrated enhanced electrochemical properties as supercapacitors. The ZnOL@MpEG hybrids are promising for application in supercapacitors, displaying a high specific capacitance of 347 F g^{-1} at a current density of 5.0 A g^{-1}.

2. Overview and history of graphene-based metal oxide NCs

Since the 1990s, after the discovery of 0D buckminsterfullerene, other carbonaceous materials, *e.g.* fullerenes and CNTs, have attracted great interest because of their extraordinary mechanical and electronic properties. Formerly, it was proposed fullerene and CNTs can be derived from 2D graphene sheet. Nevertheless, as a matter of fact, they are not obtained from graphene, successively increasing the interest in research field of carbon-based materials.[116] The discovery of graphene revolutionized and thoroughly redefined leading-edge technology with its exceptional thermal, mechanical, electronic and optical properties. Owing to these outstanding properties, graphene has been explored as major filling agent in NCs, where it can strengthen and improve the interfacial bonding between the host matrix and graphene.[117] As far back as the 1840s, graphite oxide and graphite intercalation compounds were explored, which were precursor materials used primarily to obtained graphite nanoplatelets and graphene-based materials. However, many studies have been focused on the use of graphene derivatives (GO, rGO, frGO, *etc*) as alternatives to pristine graphene because of its high production cost. There are three different historical method for the synthesis of GO dating back to 1958.

The first reported method was the Brodie technique, where $KClO_3$ was added to a graphite and fuming HNO_3 mixture, achieving the oxidation of graphite. Later, the Staudenmaier technique was developed, which is a modified Brodie method replacing HNO_3 with a mixture of concentrated H_2SO_4 and HNO_3. Thirdly, the Hummer's method was reported, where $KMnO_4$ was added to a solution of $NaNO_3$ and H_2SO_4. However, this method releases toxic gases, namely NO_2, N_2O_4 and explosive ClO_2. Thus, to control their release, an improved Hummers' method was investigated by the Tour group at Rice University by excluding $NaNO_3$ for the environment-friendly synthesis of GO.[118] Boehm *et al.* reported the use of various chemical reductants (such as hydrazine and hydroquinone) as well as thermal expansion and reduction of a GO dispersion.[119] However, the toxicity of these chemical reducing agents poses a major risk to living organisms and the ecosystem. Thus, to overcome these issues, researchers recently reported an easy, cost effective and eco-friendly green alternative for reduction. Scientists reported a green synthesis method using plant extracts, fruit extracts, microbes, metal powder, vitamin C, organic acids, carrot juice, coconut water, and green tea.[120–122]

A variety of applications has been envisioned for the use of graphene and graphene derivatives as reinforcing nanofillers. The advancement in the field of graphene-based NCs has been outlined in numerous review and research articles, either by considering particular materials including inorganic materials or polymers or specific applications for energy and environment.[116] In the past few decades, most of the literature published on NCs of graphene with metal oxides and polymers reported a remarkable enhancement in their structural as well as functional properties. To date, different types of metal oxides including ZnO, MnO_2, SnO_2, TiO_2, Fe_2O_3, Fe_3O_4, NiO, Co_3O_4, and Cu_2O[123] have been prepared and incorporated in graphene. Notably, very limited literature has been reported on NCs of group-5 elements such as niobium and tantalum. Furthermore, sometimes transition metals are also added to graphene-based metal oxide NCPs of indium and tantalum.[124] Similarly, Wang *et al.*[125] reported the preparation of NCs of graphene with metal oxides (SnO_2, NiO, MnO_2 and SiO_2) and their potential in energy storage was demonstrated. SnO_2/graphene NCs films exhibited a near theoretical specific energy density for Li-ion insertion without notable charge/discharge degradation. The NCs of TiO_2, Mn_3O_4, and Co_3O_4 with rGO exhibited potential application in lithium-ion batteries.[126] NCs of graphene with metal oxides have attracted extreme interest from researchers for the fabrication of well-organized supercapacitors. Anwar *et al.*[127] in their research article described the supercapacitor behavior of graphene-based metal oxide (CO_3O_4, Cu_2O, Fe_2O_3, Fe_3O_4, V_2O_5, MnO_2, TiO_2, NiO, $Ni(OH)_2$, RuO_2, SnO_2, WO_3, and ZnO) NCs. In their literature review, they also analyzed that nickel NCs poses a greater specific capacitance, while NCs with different forms of manganese exhibit higher relative stability. Zhang *et al.*[128] in their feature article reviewed the electrochemical performance of NCs of graphene NSs with A_3O_4-type transition metal oxides (A = Mn/Fe/Co). The electrochemical properties of the synthesized NS-based Mn_3O_4, Fe_3O_4 and Co_3O_4 were investigated by cyclic voltammetry and galvanostatic charge–discharge tests. They exhibited a high energy density (20, 10 and 7 W h kg^{-1}), large specific conductance (708, 358 and 240 F g^{-1}) and good electrochemical stability (73%, 67.8% and 95.8%), respectively.

Graphene and metal oxide/polymer NCs have promising application as photocatalysts due to the advanced arrangement of their electronic structure, charge separation and transport and light absorption properties. A major breakthrough in photocatalysis research was reported in 1972, when Fujishima and Honda discovered that TiO_2 together with a Pt electrode enabled the electrochemical photocatalysis of water under UV light radiation.[114] A variety of inorganic nanoparticles including TiO_2, CuO, BiOCl, ZnO, CdO, CdS, $ZnWO_4$, SnO_2, $NiFe_2O_4$, Bi_2O_3/BiOCl, and $MnFe_2O_4$ has been proposed to poses photocatalytic activity. However, they are associated with a few drawbacks such as poor absorption capacity, fast electron–hole recombination, low photocatalytic quantum yield, and low stability. Thus, various approaches have been employed to improve the photocatalytic performance of graphene NCs such as surface sensitization, doping, improving their electrical conductivity, increasing the number of catalytic active sites, coupling, constructing well-ordered NSs, and fabrication of different structures. Singh *et al.*[129] discussed all these modification pathways briefly in their review. Functionalized graphene-reinforced metal oxide/polymer NCs have been shown to be promising in environmental sensing and remediation. Also, the photocatalytic activities of TiO_2 NPs have been reported to be increased by the incorporation of graphene. Zhang *et al.*[130] employed graphene/TiO_2 NCs as a photocatalyst for the degradation of organic dyes such as methylene blue. Graphene/TiO_2 showed the better photodegradation of dyes compared to CNTs/TiO_2 and pure TiO_2 due to the efficient charge separation and extended light absorption properties of graphene/TiO_2 NCs. Besides TiO_2, graphene NCs with ZnO and Cu_2O were also explored for the photodegradation of pollutants.

3. Synthesis of graphene oxide nanosheets

In the synthesis of GO, the choice of graphite is important. Brief accounts on the reported processes are presented in the following sections. There are four methods for the synthesis of graphene oxide, as follows:

(1) Synthesis of graphene oxide from graphite flakes.
(2) The original Hummers' method.
(3) Two-step modified Hummers' method.
(4) The improved Hummers' method/one-step modified Hummers' method.

Herein, we discuss the synthesis of GO by different methods and the most recent method for its synthesis, *i.e.* improved Hummers; method/one-step modified Hummers' method.

3.1. The original Hummers method

Generally, graphene oxide is synthesized by the Hummers' method (HM)[131] and improved modified Hummers' method (MHM)[132] (Fig. 5). In the Hummers' method, graphite is subjected to the oxidation process using sulphuric acid, sodium

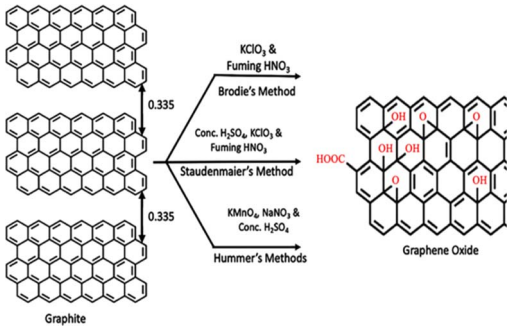

Fig. 5 Representation of the synthesis of GO using different methods with the production of under an oxidized hydrophobic carbon material.

nitrate, and potassium permanganate (while hydrogen peroxide is used for the elimination of permanganate and manganese dioxide residue), which produces a bright-yellow colour suspension, and also terminates the reaction. The bright-yellow colour confirms the conversion of GO from pristine graphite. Sulphuric acid provides acidic condition in the reaction, while $KMnO_4$ acts as a strong oxidizing agent in acidic condition. When $KMnO_4$ is added to the sulphuric acid-containing pristine graphite, graphite is inserted in sulphuric acid. This results in the growth of graphite bisulfate ions, in which each single-layer of graphene is inserted through different layers of bisulphate ions.[133,134] This effective intercalation facilitates the successful diffusion of $KMnO_4$ into the graphene layers for the oxidation of graphite.

The modified improved Hummers' method is either a one-step method or two-step method. The one-step modified Hummers' method was developed by Chen *et al.*[89] In this method, also known as the "improved Hummers'" method, $NaNO_3$ is not used in the oxidation process. Alternatively, in the two-step modified Hummers' method, H_2SO_4, $K_2S_2O_8$ and P_2O_5 are used for the pre-oxidation of graphite powder. Then, the pre-oxidized graphite is exposed to oxidation using $KMnO_4$ and H_2SO_4 by the Hummers, method. Marcano and co-workers[135] developed a new method for the synthesis of GO, which they called the "improved synthesis" of GO. They used $KMnO_4$ in a weight ratio of 9 : 1 with an H_2SO_4 and H_3PO_4 mixture. In addition, Xu *et al.*[136] developed another approach called "mild oxidation" by reducing the $KMnO_4$/graphite ratio from 3 : 1 to 1 : 1.

4. Synthesis of reduced graphene oxide (rGO)

The reduction of GO can be accomplished by different approaches including chemical, electrochemical, thermal,[137,138] and photochemical methods[139] to achieve graphene-like materials, which are generally referred to in the literature as highly reduced graphene oxide (HrGO), reduced graphene oxide (rGO), chemically reduced graphene oxide (CrGO), chemically converted graphene (CCG), *etc.*

4.1. Chemical methods

Chemically reduced graphene oxide or graphene using GO by applying different reducing agents such as $NaBH_4$, hydrazine monohydrate, and many other chemicals.[140–143] Among the reducing agents, hydrazine is the most significant and undoubtedly the most reported and extensively used reductant owing to its excellent stability and reactivity in aqueous medium. The reduction of GO through hydrazine reestablishes the π-conjugation inside the aromatic rings in graphite, resulting in an enhancement in electrical conductivity. Previously, the hydrazine-mediated reduction of graphene oxide was observed to yield the highest conductivity of about 99.6 S cm^{-1} and the C/O ratio was estimated to be 12.5; however, an electronic conductivity of up to 300 S cm^{-1} was perceived with the less noxious acetic acid and hydroiodic after replacing hydrazine.[144,145] Although hydrazine efficiently eliminates oxide functional groups, it also leads to the addition of impurities such as nitrogen, which remains covalently bound on the surface of the graphene sheets in the form of hydrazones, amines, or other functionalities.[141] Furthermore, it has been described that higher features of graphene can be achieved by reducing GO with hydrogen gas, but the requirement of inert condition and high temperature restricts its applications.

4.2. Thermal methods

GO can be reduced by another operative technique, *i.e.*, thermal method, where it can be prepared by the thermal exfoliation of graphene oxide followed by rapid heating (>200 °C min^{-1}) of dehydrated GO under an inert atmosphere at high temperature (about 1050 °C).[146] The quick heating of GO leads to the breakdown of the oxygen moieties convoluted on the GO plane of carbon, releasing poisonous gases such as CO and CO_2. The free gas gradually evolves into the space present between the GO sheets and produces local pressure within the stacked layers, which ultimately aids the exfoliation process of GO. This thermal treatment not only exfoliates but also reduces GO to graphene, concurrently by eliminating oxygen-containing moieties, which is referred to as TRG (thermally reduced graphene). In the exfoliation process of GO, about ~30% mass loss of GO occurs due to the disintegration of the oxygen-containing moieties and dehydration of water. Thus, these techniques only produce small-size and wrinkled graphene sheets with severe topological defects and the TRG sheets are damaged with etches holes all over the plane of the sheets.[147] These defects reduce the carrier transport path length, and also induce numerous smattering spots in the TRG sheets, which shows adverse effects on their electronic properties.[148]

However, although the thermal reduction techniques of GO are exceedingly effective, more efforts are required to attain the high-quality large-scale production of rGO at lower calcination temperatures. In essence, high-temperature annealing not only requires critical treatment conditions, but also needs larger energy consumption and demands sophisticated and expensive instruments. Moreover, the fabrication of HRG films on substrates containing inorganic/organic materials is difficult

under the thermal reduction conditions, which requires electronic instruments for annealing at high temperature.

4.3. Microwave-assisted method

GO reduction by the microwave method involving high-temperature galvanizing is extremely effective and extensively applied, but it poses some noticeable disadvantages.[149] Thermal annealing is generally carried out by thermal treatment; nevertheless, some unusual heating instruments have been studied for thermal reduction, such as microwave irradiation (MWI).[150,151] In this technique, microwave energy is converted into heat. Compared to other established heating approaches, the reaction solution is homogeneously and speedily. Moreover, the reactant and solvent possess different dielectric constants, and therefore, selective dielectric heating throughout the reaction can be carried out by the MWI method. Recently, MWI has revealed admirable capacity to synthesized graphene from GO. However, the interaction between GO graphene with microwaves is not fully understood to date.

Hu *et al.* described that for carbon-based materials, their MW assisted synthesis mostly relies on their chemical structures and configuration. In this study, the oxygen content in the GO and graphene materials was varied, where the absorption capability of GO was reduced remarkably with an increase in oxygen moieties because of the decrease in the sp^2 hybridized structure. Moreover, the GO reduction process was speculated due to the small addition of pristine graphene, which was greatly enhances. Exfoliated graphite (EG) was preparing by this MWI method using a variety of graphite-intercalating graphite compounds (IGCs).[152] EG was also synthesized by MWI very quickly (4 min); where a mixture of natural graphite and $KMnO_4$ and HNO_3 was directly heated in a microwave oven. The preparation of rGO also been described by concurrent GO exfoliation and reduction under a dry environment by rapid MWI in ~1 min.[153]

4.4. Hydrothermal and solvothermal methods

The hydrothermal method is an extraordinary, potent and incipient chemical reduction process for the green fabrication of graphene and graphene-based composites.[149] This one-step method can be employed to synthesize highly uniform crystalline NSs without further annealing/calcination process.[154] The reduction of GO by the hydrothermal process is carried out in a sealed tube system in the presence of either water or a solvent (solvothermal process) at a certain temperature or beyond its boiling point to generate extremely high reduced pressure.[155] Supercritical water (SCW) is considered an ecofriendly reducing agent and alternative to noxious chemical reducing agents. GO reduction can be achieved hydrothermally *via* SCW, where SCW not only removes the oxygen-containing functionalities partially but also recovers the aromaticity of the compound.[156] During this reaction, SWC acts as a source of protonated H^+ ions for the hydroxyl groups. This leads to the dehydration of rGO, thereby simplifying the reduction method. Moreover, the true pH may be different compared to other reduction procedures. The minimal pH of the solution plays an important role, *i.e.* a basic solution (pH = 11) yields a constant rGO solution, while the rGO sheets aggregate in an acidic solution (pH = 3).

GO deoxygenation was carried out by solvothermal reduction. In this procedure, Wang *et al.* describes the reduction of GO using *N*,*N*-dimethylformamide (DMF) as the solvent at 180 °C and hydrazine monohydrate as the reducing agent.[157] The rGO sheets were dispersed in DMF solvent, and the C/O ratio in the rGO sheets reached 14.3. However, the presence of nitrogen doping initiated by hydrazine resulted in poor conductivity in the rGO sheets. In a different study, Dubin *et al.* used *N*-methyl-2-pyrrolidinone (NMP) as the solvent for the solvothermal reduction reaction.[158] Here, a sealed tube container was not used for the reduction of GO and the reaction temperature was less than (200 °C) the boiling point of NMP (202 °C at 1 atm). It was suggested that the oxygen-scavenging properties of NMP at higher temperature and the adequate thermal annealing aided the reduction of graphene oxide.[159]

4.5. The green reduction of graphene oxide

In a distinctive reduction of GO, firstly a GO suspension dispersed in an appropriate solvent and ecofriendly green reducing agents are blended to yield the reaction solution and *in situ* binding. Furthermore, under controlled different temperatures and altered times, the reaction mixture was preserved. In previous studies, the concentration of GO was about 0.1–1 mg mL^{-1}, and the temperature of the reaction was observed to be 80–85 °C. Table 1 shows the GO concentration, temperature and reduction time of GO in different reports. The pH is a vital parameter for the reaction solution because a change in the pH will possibly change the reduction process in different solutions, *i.e.*, both acidic and alkaline media.[160] Especially, HCl, NH_4OH and dilute NaOH are used to control the pH of the reaction solution.[161] Merino *et al.* discussed that alkaline solution is vital for the reduction process in a shorter time. Therefore, the further use of any reducing agent can deoxygenate the GO sheet.[162] It increases the colloidal durability of the GO sheet due to electrostatic repulsion. Bosch *et al.*[163] clearly demonstrated that graphene sheets are affected by the use of different pH solutions. According to their conclusions, for large defects, acid pH is responsible for a higher concentration, extensive agglomeration and small size reduction of graphene sheets. An acidic pH may turn the graphene into others forms of graphite with a nano-size, for instance fullerene, nano-flowers, nano-onion and MWCNTs. This study disclosed that alkaline pH is more favorable for the fabrication of less defective and high-quality graphene.[164] After the reduction, the GO solution turns from a brownish-yellow colour into a black slurry of graphene sheets. The obtained graphene sheets are extracted either filtration or by centrifugation.[165] After centrifugation, the obtained black slurry should be washed numerous times with deionized water and alcohol to remove all the unwanted materials. After carrying out the washing process, the pH of the slurry should be neutral (pH = 7).[166] Lastly, the solid and black rGO sediment can be dried in a vacuum oven at 50–100 °C.[167]

Xiao *et al.*[168] synthesized functional graphene nanosheets, which were dried at room temperature. In this report, L-valine

was used for the reduction of GO to rGO as a green biomolecule source. Furthermore, the quality of the functional graphene sheets vastly depend on the following features: (i) the properties of the original graphite, (ii) process of oxidation, and (iii) final deoxygenation method of GO to graphene.

Feng *et al.*[141] established an ecofriendly technique for the large-scale fabrication of high-quality rGO with a small content of oxygen. A reducing agent Na-NH_3 solution were used, where the solvated electrons assisted the GO reduction and the construction of a conjugated complex of rGO with an oxygen content of 5.6 wt%. Recently, Esfandiar *et al.*[169] reported the

Table 1 Summary of process settings in the reduction of graphene oxide by plant extracts/bacteria/fungi/yeast

Reducing agent	Time	Temp (°C)	GO (mg mL^{-1})	Ref.
L-Valine	A few h	90 °C	0.1	168
Melatonin	3	40 °C, 60 °C, 80 °C	0.1	169
Aluminium powder	3	100 °C, 200 °C	4	170
Pulicaria glutinosa	24 h	98 °C	5	173
Dalbergia latifolia				174
Gallic acid	24	RT	4	175
Carrot root	48	RT	0.5	176
Shewanella cells	48	RT	300	177
P. aeruginosa	72 h	37 °C	0.35	178
Asian red ginseng	10 min	80 °C	0.1	179
Syzygium aromaticum	30 min	100 °C	1.6	180
Chinese wolfberry	24 h	90 °C	0.5	181
E. coli	48 h	37 °C	5	182
Yeast	72 h	35–40 °C	0.5	183
Caffeic acid	12 & 24 h	95 °C	0.1	184
Hibiscus sabdariffa	1 h	—	0.4	185
Allium sativum	3 h	100 °C	5	186
Eichhornia crassipes	10 h	180 °C	0.1	187
Spinach (*Spinacia oleracea*)	30 min	RT	1.6	188
Seed extract of *T. chebula*	24 h	90 °C	1	189
Grapes (*Vitis vinifera*)	1, 3, 6 h	95 °C	0.6	190
Salvadora persica roots	24 h	98 °C	5	191
Pomegranate juice	12, 18, 24 h	60 °C	2.5	192
Caffeine	12 h	80 °C	0.1	193
Cinnamomum verum	12 h	100 °C	1	194
Chrysanthemum	24 h	95 °C	0.1	195
Ficus religiosa	24 h	50 °C	0.1	196
Mangifera indica	24 h	70 °C	N/A	197
Mangifera indica L.	8 h	70 °C	1	198
Azadirachta indica	60 min		11.1	199
Green tea extracts	8 h	80 °C	0.5	200
β-Carotene	24 h	95		201
Cinnamon	45 min	RT	1.6	202
Cocos nucifera L.	12, 24, 36 h	100 °C	0.66	203
Curcumin	120 min	85 °C		204
Tea polyphenols	8 h	80 °C	1	205
Tea polyphenols + iron	10 min	40 °C, 60 °C, 80 °C	0.1	206
Rosa damascena	5 h	95 °C	7	207
Sugar cane juice	12 h	150 °C	1.25	208
Marigold flower	3 h	95 °C	0.625	209
Ficus carica	24 h	80 °C	5	210
Lignin	8 h	90 °C	1.0	211
Annona squamosa	12 h	100 °C	0.4	212
Lemon extract	24 h	95 °C	0.1	213
Platanus orientalis	10 h	100 °C	1	214
Cherry, *Magnolia, Platanus*	12 h	95 °C	0.5	215
G. biloba		30 °C	0.5	216
Rose water	5 h	95 °C	7	217
Reducing sugar	1 h	95 °C	0.1	218
Tin powder	0.5–3 h	RT	1	219
Vitamin C	0.5–4 h	95 °C	0.1	220
L-Ascorbic acid	N/A	23 °C	0.1	221
L-Cysteine	12–72 h	26 ± 2 °C	0.5	222

reduction of GO by introducing melatonin as a replacement for hydrazine. Melatonin is a biocompatible antioxidant, which led to excellent results compared hydrazine under the same conditions. Moreover, due to the π–π stacking of the melatonin molecules on the reduced graphene sheets, the melatonin-reduced suspension of GO suspension was more stable compared with the hydrazine-reduced suspension, this is due to its greater aggregation.

Newly, metal-based GO reduction has been considered eco-friendly and leads to more rapid reduction of GO. Fan *et al.* described an efficient synthesis technique for the reduction of GO using aluminum powder.[170] The reaction was completed within a short time of less than 30 min under the acidic medium. The graphene sheets showed a high bulk electrical conductivity of 2.1×10^3 S m^{-1}. Similarly, Mei and Ouyang replaced Al with Zn, leading to the successful reduction of GO using the sonication method at room temperature in mild acidic medium.[171] The reaction was completed in one minute, *i.e.* taking much less time than described for GO reduction using aluminum and with iron powder. The low reduction potential of Zn^{2+}/Zn and ultrasonication facilitated the fast and efficient reduction of GO. Furthermore, the rGO sheets achieved by this technique displayed good electrical conductivity and effective thermal stability.

More recently, there has been a new trend of employing plant extracts that can act as reducing/capping/stabilizing agents during the synthesis of nanoparticles, where this property of plant extracts has fascinated noteworthy attention of the scientific community. Plant extracts (PE) are comparatively easy to handle, easily available, cost effective, and have been significantly exploited owing to their biocompatibility in the field of nanoscience and nanotechnology. Although different metallic NPs have been previously synthesized effectively using PE as bioreductants,[172] their reducing capacities have been tested recently for the reduction of GO to rGO.

Khan *et al.* demonstrated the *Pulicaria glutinosa* (*P. glutinosa*) plant extract (PE)-assisted green synthesis of HRG *via* GO using efficient green root. The phytochemicals present in the PE of *P. glutinosa* were responsible for the reduction of GO and also functionalized the HRG nanosheets to stabilize different solvents on their surface, which eliminated the need for other harmful surfactants and reductants (Fig. 6).[173] Nagaraj *et al.* developed a green route for the biosynthesis of rGO *via* a green approach using *Dalbergia latifolia* leaf extract act as a reducing, capping and stabilizing agent for the reduction of GO.[174] Similarly, Li *et al.* described a green method employing gallic acid for the reduction of GO, which acted as both a stabilizing and reducing agent in the reduction process.[175]

Besides this, the microbial reduction of GO is a new trend that has widely been reported. Kuila *et al.* reported the carrot root-based reduction of GO to HRG. Here, the endophytic microorganism present in the carrot root acted as a biocatalyst, which helped the reduction to proceed at room temperature.[176]

Similarly, Wang *et al.* demonstrated the reduction of GO *via* the microbial inhalation of Shewanella cells under ambient condition in an aerobic experimental setup.[177] Due to the metal-reducing property of Shewanella bacteria, they metabolically generate electrons, which transfer to the external parts of the metal oxide solids from the interior parts of the cells. In the GO reduction process, the extracellular electron transfer is mediated by both the self-secreted electrons and outer membrane containing c-type cytochromes (Mtr/Ornc). It has been described that microbially reduced GO possesses admirable electrochemical properties compared with that synthesized by chemical methods. Similarly, Potbhare *et al.* employed bacterial biomass extract (*Pseudomonas aeruginosa*) for the reduction of graphene oxide as well metal salts. The biomass extract acted as a stabilizing and reducing agent in the reaction.[178]

5. Synthesis of graphene-based metal oxide nanocomposites (GMONCs)

The anchoring of metal/metal oxides NPs on graphene sheets for the fabrication of graphene-based NCs can generally be performed *via* two different methodologies (Fig. 7), *i.e.*, *ex situ* hybridization and *in situ* binding. *Ex situ* hybridization involves the mixing of separate pre-synthesized NPs and graphene sheets. Before blending both the NPs and graphene sheets, their surface functionalities can be enhanced using the sonication approach.[223] The non-covalent π–π stacking and/or covalent C–C coupling reactions facilitate the functionalization of the conjugated graphene sheets. The functionalization of graphene-

Fig. 6 Green reduction of graphene oxide (GO) using an aqueous leaves extract.

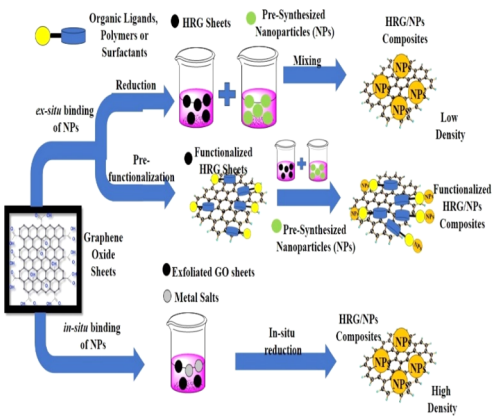

Fig. 7 Schematic illustration of the binding mechanisms of NPs on HRG sheets.

based NPs significantly enhances their solubility, facilitating the fabrication of graphene-based NCs. However, *ex situ* hybridization may result in the non-uniform distribution of NPs on the graphene sheets, which may also suffer from a low density. In this review, we discuss the *in situ* crystallization method for the fabrication graphene-based metal oxide NCs. In following sections, we present the most recent techniques for the fabrication of graphene/metal oxide NCs. Readers interested in the details of the *in situ* methods (*e.g.* functionalization and preparation of functionalized graphene-based metal oxide NCs) can refer to the brilliant reviews by Yang or Shi *et al.*[223,224]

Different methods can be applied for the preparation of graphene-based metal/metal oxide NCs by *in situ* combining metal precursors such as $AgNO_3$, $HAuCl_4$, H_2PdCl_6, and K_2PtCl_4 with reductants such as $NaBH_4$, hydrazine hydrate, and amines, which are commonly and widely applied. Alternatively, the preparation of NCs *via* the green reduction of metal/HrGO is a straightforward, cost-effective and single-pot method, and thus researchers are currently focused on finding green reducing agents for the fabrication of graphene-based NCs. A summary of the diverse graphene-based metal oxide NCs is given in Table 2. In this context, the green synthesis of Ag/HrGO

Table 2 Summary of diverse graphene-based metal oxide NCs

Graphene-based metal oxide	Method of synthesis	Graphene filler	Ref.
ZnO/rGO	Co-precipitation	rGO	227
rGO/SnO_2/Au	Co-precipitation	rGO	228
Pd@graphene	Co-precipitation	Graphene	229
Graphene-TiO_2	Sol–gel	Graphene	230
rGO-SiO_2	Sol–gel	rGO	231
Graphene-$BiFO_3$	Sol–gel	Graphene	232
TiO_2-graphene	Sol–gel	Graphene	233
ZnO@rGO	Microwave	rGO	237
rGO/TiO_2	Hydrothermal	rGO	238
g-Fe_3O_4/rGO	Hydrothermal	rGO	240
rGO-ZnO	Hydrothermal	rGO	242
MO-chitosan-GO	Solution cast	GO	243
rGO-Fe_3O_4	Co-precipitation	rGO	244
NiO/rGO	Bath deposition	rGO	245
Graphene/Mn_3O_4	Solvothermal	Graphene	246
rGO/WO_3	Ultrasonication	rGO	247
rGO/NiO	Decomposition	rGO	248
Fe_3O_4/ZnO-rGO	Dry method	rGO	249
Graphene/Pd/TiO_2	Hydrothermal	Graphene	250
CuO–ZnO-Fe_2O_3/rGO	Co-precipitation	rGO	251
Graphene-Mn_2O_3	Sonochemical	Graphene	252
Graphene-TiO_2/Fe_3O_4	Solvothermal	Graphene	253
$ZnFe_2O_4$/graphene	Hydrothermal	Graphene	254
ZnO-rGO	Microwave	rGO	255
β-$SnWO_4$-rGO	Microwave	rGO	256
Ag-Cu_2O/rGO	Co-precipitation	rGO	257
Fe-doped TiO_2	Sol–gel	rGO	258
rGO@CuO	Co-precipitation	rGO	259
Ce-Bi_2O_3-rGO	Co-precipitation	rGO	260
MnO_2/graphene	Hydrothermal	Graphene	261
Cu/$Bi_2Ti_2O_7$/rGO	Co-precipitation	rGO	262
GO-modified TiO_2	Hydrothermal	GO	263
Co_3O_4/TiO_2 GO	Sol–gel hydrothermal	GO	264
Fe_3O_4/Mn_3O_4-rGO	Polyol	rGO	265
$Ce(MoO_4)_2$/GO	Hydrothermal	GO	266
ZnO-G/TiO_2-G	Hydrothermal	Graphene	267
Co/GO-TiO_2	Sol–gel	GO	268
Fe_3O_4/rGO	Co-precipitation	rGO	270
Graphene-$LiMn_2O_4$	Solvothermal	Graphene	271
V_2O_3/rGO	Solvothermal	rGO	272
SnO_2/rGO	Hydrothermal	rGO	273
$ZnFe_3O_4$/GO/Chitosan	Solution mixing	GO	275
rGO/ZnO	Co-precipitation	rGO	276
Graphene/$Ni_3V_2O_8$	Solvothermal	Graphene	277
ZnO–CuO/N-rGO	Hydrothermal	rGO	278
SnO_2/Co_3O_4/rGO	Co-precipitation	rGO	279
Fe_3O_4 NPs/N-rGO	Hydrothermal	Graphene	280
Co_3O_4 NR/RGO	Hydrothermal	rGO	281

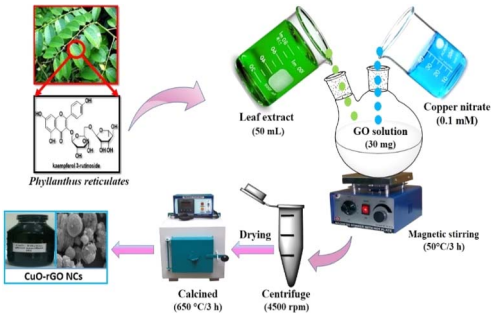

Fig. 8 *Phyllanthus reticulatus*-mediated photosynthesis of CuO-rGO NCs.

is effective and environmentally friendly, where the *in situ* reduction process occurs by simultaneously adding both GO and $AgNO_3$ in aqueous solution using tannic acid (as a green reducing agent).[225] The obtained material demonstrated exceptional SERS (surface enhanced Raman scattering) activity as an SERS substrate, and remarkable catalytic property for the reduction of hydrogen peroxide.

Metallic NPs can be anchored to the surface of rGO sheets *via* two techniques, *i.e.*, *in situ* and *ex situ* binding. A bulk yield of NPs can be achieved through *in situ* binding. Both rGO sheets and NPs can be functionalized either by C–C coupling covalent reactions or non-covalent π–π stacking. In addition to bimetallic NPs, graphene-based metal oxide NCs have been fabricated by *in situ* binding *via* bioinspired reduction (Fig. 8).[226]

5.1. Co-precipitation method

Elavarasan *et al.*[227] demonstrates an economical and sustainable approach for the biogenic synthesis of ZnO/rGO NCs *via* a simple co-precipitation method using aqueous leaf extract of *Dalbergia latifolia*. TEM revealed that the typical particle size of the ZnO/rGO NCs was 12–18 nm, which were arbitrarily anchored on the edges and surfaces of the GO NSs. This study revealed the potential anticancer activity of the synthesized NCs on the MCF-7 cell line compared to the A-549 cancer cell line. Furthermore, the results indicated that the metal oxide NPs with graphene as excellent chemotherapeutic agents may have an even wider variety of applications in the treatment of cancer.

rGO/SnO_2/Au nanohybrid materials were fabricated using a dispersion of GO and $SnCl_2$ aqueous solution by Meng *et al.*[228] $SnCl_2$ acted as a reducing agent in the reaction, which is the key step of the synthesis, and tin reduces both GO and $HAuCl_4$ by the sonication-assisted method. This approach also has the potential for preparing other multicomponent NCs using different metal precursors.

Al-Marri *et al.*[229] successfully synthesized palladium NPs loaded on graphene sheets *via* a green method using *S. persica* L. (*miswak*) root extract as a bioreductant. Using this technique, spherical and crystalline palladium NPs were homogeneously scattered on the surface of graphene sheets owing to the superior dispersibility of the synthesized NCs by the stabilization of the phytomolecules in the *S. persica* L. (*miswak*) root extract, where the as-prepared NCs exhibited outstanding catalytic properties toward the oxidation of different aromatic alcohols.

5.2. Sol–gel method

The sol–gel method enables the straightforward and economical synthesis of uniform NC materials with admirable compositional control, and therefore is used in many applications. Zhang and coworkers prepared graphene-TiO_2 NCs *via* the sol–gel approach, where graphene oxide and tetra butyl titanate were employed as the starting materials and the fabricated NCs showed photocatalytic activity, which was affected by both the calcination temperature and graphene content.[230] Hintze *et al.* fabricated rGO-SiO_2 NCs using the sol–gel method, having a controlled carbon phase with significant electrical conductivity.[231] Sol–gel-mediated graphene-$BiFO_3$ NCs were synthesized by Nayak *et al.* and their electrochemical performance as a supercapacitor investigated. Graphene-$BiFO_3$ NCs exhibited a specific capacitance of about 17–4 mF cm^{-2} and 95% retention of capacitance after 2000 cycles.[232] Li *et al.* developed a sol–gel method for the synthesis of ultra-disperse TiO_2 NPs on the surface of graphene sheets with extreme control, enabling the developed nanomaterial to achieve two times the specific capacity of mechanically mixed NCs.[233]

5.3. Microwave-assisted method (MWI)

MWI is broadly used for the preparation of graphene-based NCs.[234] Mostly, the *in situ* reduction of rGO/metal oxide NCs using GO and various metal precursors is highly effective. MWI techniques have attracted increasing attention due to their scalable and large-scale production, and also easy processing. Moreover, the fast and uniform heating by microwaves inhibit the agglomeration of the graphene layers. However, the major drawbacks of this technique are the poor homogeneity and distribution NPs on the surface of rGO sheets and inability to control the NPs size. Hassan *et al.* demonstrated that rGO/bimetallic NP composites can be prepared *via* the reduction of GO using the microwave technique.[235] This method permitted the speedy chemical reduction of graphene oxide with a variety of reducing agents in both aqueous and organic solvents, where the instantaneous reduction of the metal salts and led to the formation of graphene sheet-supported metallic and bimetallic NPs. Dey *et al.*[236] developed a novel, economical and green route for the *in situ* reduction of graphene/iron oxide NCs (GINC). An efficient material with an enhanced thermoelectric performance was developed using microwave irradiation. The fabricated NC film demonstrated a conductivity of 2.18×10^4 S m^{-1} with a Seebeck coefficient of 38.8 μV K^{-1}. Hence, the power factor (PF) reached 32.90 μW m^{-1} K^{-2}, which was folds higher than that of the thermoelectric material based on a PVAc-graphene composite. R. Kumar *et al.*[237] successfully synthesized microwave-assisted ZnO NPs and loaded them on the surface of rGO NSs to produce ZnO@rGO, which was investigated as a supercapacitor electrode. This electrode showed a specific capacitance of 102.4 F g^{-1} at 30 mV s^{-1}. Also, its cycling stability was demonstrated using CV for 3000 cycles, where its capacitance retention was maintained at 82.5%.

5.4. Hydrothermal method

Hydrothermal or solvothermal reduction techniques have been widely applied for the fabrication of graphene-based metal oxide NCs.[238] Hydrothermal treatment is not only preferred for the reduction of GO but also aids in the synthesis of metal oxide NPs. It becomes clear that hydrothermally fabricated graphene materials can be produced in large quantities with acceptable structures and properties. These techniques have numerous benefits. For example, the inexpensive raw material graphite is used for the production of graphene-like materials (rGO) on a large scale, making them very economical. Graphene/rGO achieved from hydrothermal methods is exceedingly processable and can be used for the production of devices and macroscopic nanostructures on a large scale *via* simple, economical and green reduction methods. Hence, these methods have gained noteworthy consideration by the scientific community, and the hydrothermal route is considered an exceptional tool for widespread research in the future. It is a big challenge to entirely eliminate the functional moieties from the surface of rGO sheets, and the restoration of the defects formed during the oxidation procedure is very challenging.

Recently, Shen *et al.*[239] reported the use of glucose as an eco-friendly reducing agent. It has been proposed that the reducing capability of glucose may enhance the yield of a reduced suspension of graphene (rGO) under hydrothermal conditions analogous to that acquired with hydrazine. The process of reduction was complemented by the construction of rGO/TiO_2 NCs, whereas the photocatalytic efficiency of TiO_2 NPs was superior due to the interface between TiO_2 NPs and rGO.

Padhi *et al.*[240] reported the novel, ecological, single-step *Averrhoa carambola* leaf extract-mediated fabrication of a stable photocatalyst and magnetically separable g-Fe_3O_4/rGO NCs. The hydrothermal route was adopted for the fabrication NCs, which resulted the excellent incorporation of g-Fe_3O_4 NPs with an average particle size of about 22 ± 2 nm in 2D rGO sheets. The as-fabricated NCs showed superior photocatalytic activity toward the reduction of Cr(VI) ions using 50 mg L^{-1} catalyst. Specifically, 97% degradation occurred within 1 h using 10 mg L^{-1} photocatalyst, while 76% phenol degradation was observed within 2 h a under visible light illumination at room temperature. Furthermore, the g-Fe_3O_4/rGO NCs showed better antibacterial activity towards Gram-positive bacteria compared with Gram-negative bacteria.

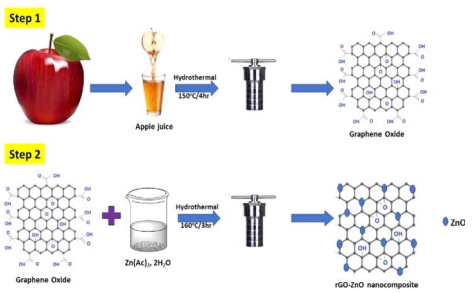

Fig. 9 Synthesis of GO and rGO/ZnO NCs *via* hydrothermal method.

Chaudhary *et al.*[241] designed the one-step *in situ* fabrication of graphene oxide-decorated ZnO NCs using the hydrothermal method. The estimated particle size from the TEM analysis was 15–20 nm, while the photocatalytic performances of NCs showed ~85% efficiency against MB dye under visible light irradiation within 70 min.

The development of *in situ* rGO-ZnO NCs using the hydrothermal method was reported by Kumbhakar *et al.* (Fig. 9),[242] where different concentrations of zinc precursors played an important role in the reduction of GO to rGO. The rGO-ZnO NCs showed ~91% photodegradation efficiency under irradiation from UV-vis light and 60% under sunlight irradiation within 60 min in comparison to other NCs.

6. Characterization of graphene-based metal oxide NCs

The morphology of rGO-Fe_3O_4 NCs is shown in Fig. 10A and B, where the presence of magnetic NPs on the crumpled silk-shaped graphene sheets suggests the formation of an rGO-Fe_3O_4 nanohybrid (NH). The TEM image (Fig. 10B) displays that the rGO sheet is translucent in nature and the Fe_3O_4 NPs are well distributed on the surface of the sheet. Meanwhile, TEM revealed the average particle size of about 20 nm, which is consistent with the SEM images. Hence, there was no apparent change in the morphological behavior of rGO-Fe_3O_4, The XRD pattern of rGO-Fe_3O_4 NCs is similar to that of graphene oxide Fe_3O_4 NCs (Fig. 10C). The central peaks at 2θ = 30.21° (220), 35.71° (311), 43.31° (400), 53.7° (422), 57.35° (511), and 62.72° (440) show the presence of Fe_3O_4 in both GO-Fe_3O_4 and rGO-Fe_3O_4 NCs.[244] The wide diffraction peaks reveal the small

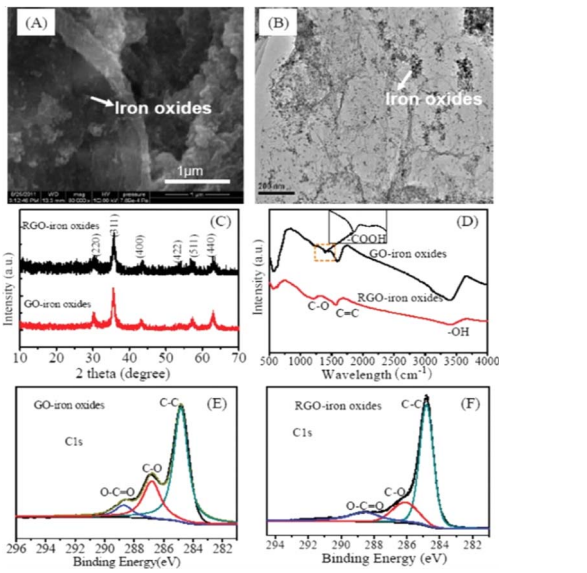

Fig. 10 SEM (A) and TEM (B) images, XRD patterns (C), FTIR spectra (D), and high-resolution C 1s (E and F) XPS of GO-Fe_3O_4 NC and rGO-Fe_3O_4 NC hybrid materials. This figure has been reproduced from ref. 244 with permission from the Royal Society of Chemistry, Copyright 2012.

crystalline size of NPs. Given that the Fe_3O_4 NPs have an analogous crystal structure to γ-Fe_2O_3, it was very difficult to differentiate them based on the XRD study. The XRD analysis revealed the presence of agglomerated graphene sheets with no carbon peak, which may be due to the fact that the magnetite NPs reduced the agglomeration of the sheets, resulting in a greater number of graphene sheet monolayers. Therefore, a weaker peak was observed for graphene and strong signal observed for Fe_3O_4 compared with the weak carbon peaks.

The FTIR spectra assisted the identification of the functional groups present in the samples. Vibration stretching bands corresponding to O–H (3389 cm^{-1}) of H_2O, C=C (1578 cm^{-1}) and epoxy C–O (1225 cm^{-1}) were observed for GO-Fe_3O_4/rGO-Fe_3O_4 NCs (Fig. 10D). In the case of GO-Fe_3O_4, an additional band was observed at 1399 cm^{-1}, which is attributed to the vibration stretching of the O–C=O group. The peak at around 584 cm^{-1} is ascribed to Fe–O, and the increased intensity for the Fe–O band is ascribed to iron anchored on GO-Fe_3O_4/rGO-Fe_3O_4.

The deconvolution of the C 1s peaks for GO-Fe_3O_4/rGO-Fe_3O_4 NCs is shown in Fig. 10E and F, respectively. The regions of the C 1s spectra could be deconvoluted into three constituents, as follows: (1) C–C (non-oxygenated) observed at 284.8 eV; (2) the C–O (carbon) peak displayed at 286.8 eV; and (3) the O–C=O (carboxylate carbon) peak, which is located at 288.8 eV. The intensity of the O–C=O peak declined in the C 1s spectrum of rGO-Fe_3O_4 as compared to that of GO-Fe_3O_4. The C/O ratio of GO-Fe_3O_4 and rGO-Fe_3O_4 is around 1.21 and 4.69, respectively, indicating that the oxygen functional groups in rGO-Fe_3O_4 were partially reduced.

The morphological exploration of NiO and NiO/rGO hybrid films were done by SEM, as shown in Fig. 11. The NiO and NiO/rGO NC films displayed superior electrochromic properties with high coloring ability, fast exchanging speed and improved cycling performance, as described by Cai *et al.*[245] The NiO NP film was porous in nature and exhibited a nanoscale interlocking network-like structure (Fig. 11a–c), which was synthesized by crumbly NiO with a particle size of about 10–15 nm. The morphological structure of both the synthesized NiO NPs and NiO/rGO hybrid film was nearly similar in nature (Fig. 11d–f). However, more open space was observed for the NiO/rGO hybrid film due to its more porous nature among all the synthesized materials, enabling the electrolyte to penetrate through the film and condense the proton dispersion tracks within the NiO bulk and the film thickness increased smoothly to 15–25 nm. The thickness of both the NP and NC films was 500 nm, as shown in Fig. 11c and f, respectively.

Qian *et al.*[246] described the fabrication of graphene/Mn_3O_4 NCs *via* the solvothermal method at 200 °C for 4 h, 8 h and 16 h, respectively, using a manganese(III) precursor. The stacking density of graphene was reduced to 70% from 100% and additionally up to 50–60%. These outcomes revealed an increase in particle size, *i.e.* 2 to 10 to 25 nm with an increase in the reaction time. The HR-TEM image revealed that the loading of the Mn_3O_4 NPs on the surface of graphene was in the crystallized form with the lattice spacings of about 0.25 nm and 0.29 nm (Fig. 12d), which are attributed to the (211) and (200) reflection planes of the tetragonal hausmannite Mn_3O_4 phase, respectively. The lattice fringes of graphene show that the number of graphene layers was about 4–5. The SAED pattern (Fig. 12e) shows deflection rings from the hausmannite Mn_3O_4 phase, with the reflection planes found to be at (112), (211), (220), (105), and (321). Fig. 12f shows the typical EDAX pattern of the graphene/Mn_3O_4 NCs, where the Mn_3O_4 NPs were anchored very well on the graphene sheet, proving the presence of Mn and O elements.

Jeevitha *et al.* synthesized porous reduced graphene oxide (rGO/WO_3) NCs. The pore size (particle distribution) and specific surface area of WO_3 with different weight percentages (wt%) of rGO content were examined using the adsorption–desorption phenomenon. Fig. 13a–c show the surface area (BET) and pore size (BJH) of the pure WO_3 and different (wt%) NCs (1% and 5%

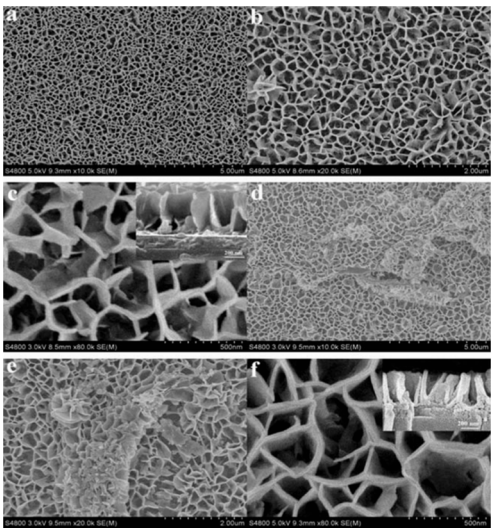

Fig. 11 SEM images: (a)–(c) porous NiO film and (d)–(f) porous NiO/rGO hybrid film. Upper-right insets in (c) and (f) correspond to the side views of the films. Reproduced with permission from ref. 245. Copyright 2012, the Royal Society of Chemistry.

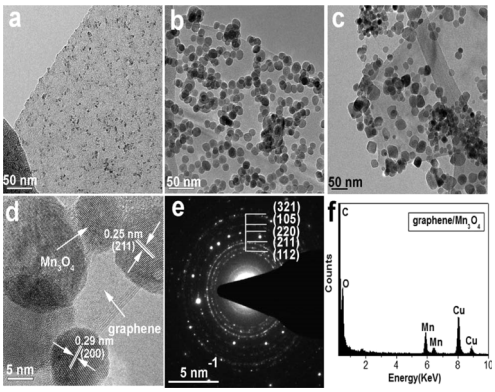

Fig. 12 TEM analysis of graphene/Mn_3O_4 NCs: products prepared at reaction times of 4 h (a), 8 h (b), and 16 h (c); HRTEM image of attached Mn_3O_4 NPs (d) and corresponding SAED pattern (e); and (f) EDS pattern of Mn_3O_4 NPs. Reproduced with the permission from ref. 246. Copyright 2017, the Royal Society of Chemistry.

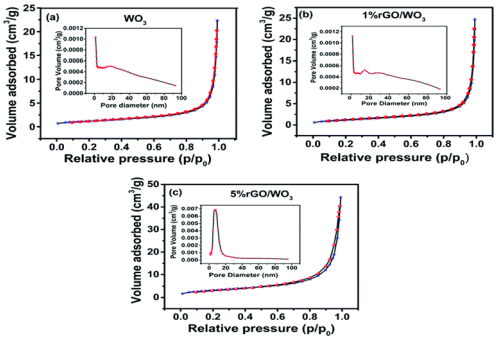

Fig. 13 Nitrogen-adsorption/desorption isotherms and corresponding pore size distribution of (a) pure WO_3, (b) 1% rGO/WO_3 and (c) 5% rGO/WO_3. This figure has been reproduced from ref. 247 with permission from the Royal Society of Chemistry, Copyright 2019.

rGO/WO_3). Astonishingly, all the samples exhibited type IV isotherms, demonstrating the mesoporous nature of the materials with a relative pressure (P/P_0) between 0.1 and 0.9. The specific surface areas of 9.96, 12.53 and 21.464 $m^2\ g^{-1}$ with an average pore size of 25.79, 31.68 and 29.41 nm were perceived for pure WO_3 and 1% and 5% rGO/WO_3, respectively.[247] This result supports the improved performance of the 5% rGO/WO_3 NCs, where the slight decrease in pore size may be due to the integration of a greater number of graphene layers.[237]

7. Photocatalytic applications

7.1. Photocatalysis

In recent years, a great deal of effort has been dedicated to solving the widespread pollution caused by effluents from urban and agricultural industries, which includes bio recalcitrant and organic pollutants.[283] in the rapid industrialization and continuous progression of newer technologies coupled with poor environmental policies have led to the generation of toxic effluents in huge amounts, which are discarded into natural water bodies. The main components of this chemical discharge from the textile, chemical, petroleum and many other industries are azo dyes. These toxic dyes not only disturb the aquatic ecosystem but also have a devastating effect on human life and the terrestrial biota. These dyes are mutagenic, carcinogenic, highly toxic to the CNS and can cause respiratory diseases, cancer, genetic disorders, chromosomal abnormalities and many acute disorders. Moreover, these dyes remain in the environment for longer periods of time without degrading.[284] Thus, in view of this situation, it has become imperative to reduce and remove these chemical pollutants (synthetic dyes) from the environment. In this regard, semiconductor-assisted photocatalysis has received global attention, given that the above-mentioned dyes are resistant to biological and physical treatment methods.[285]

Heterogeneous semiconductor photocatalysts can absorb solar radiation to generate electron–hole pairs, which can accelerate the remediation of these dyes. A simple mechanism of heterogeneous photocatalysis includes absorption of light by a semiconductor, leading to the excitation of electrons from its

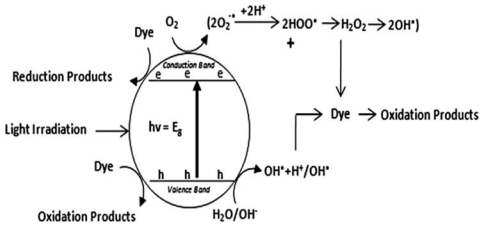

Fig. 14 Indirect dye degradation.

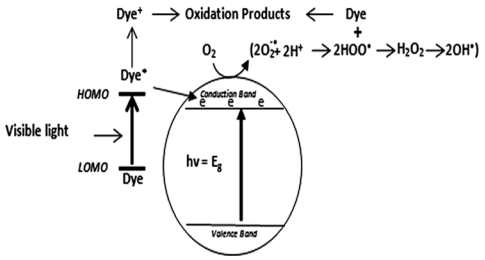

Fig. 15 Direct dye degradation.

valence band to conduction band, leaving holes in the VB. Fig. 14 and 15 depict the process of dye degradation on a semiconductor photocatalyst involving the indirect and direct pathways, respectively. In the indirect pathway, the dye is degraded by the reactive oxygen species formed on the catalyst surface. Subsequently, the photogenerated holes react with adsorbed water or hydroxyl ions to generate hydroxyl radicals, whereas the electrons in the CB react with oxygen to form superoxide radicals. These reactive oxygen species rapidly and non-selectively reduce pollutants, including dyes, antibiotics, drugs, and phenolic compounds. In the direct pathway using different sources of light irradiation, carbon-based dyes such as Rh–B, IC, TB, MO, CR and MB can also be excited in the photodegradation process, which is a phenomenon called photosensitization, and in this process, the dyes are excited from the ground state to the excited state. In the excited-state dyes, charge transfer occurs from the highest occupied molecular orbital (HOMO) to the conduction band of the photocatalyst, providing more electrons to produce superoxide radicals, significantly enhancing the photocatalytic degradation activity.[286]

However, the speedy recombination rate of photo-generated electron–hole pairs within photocatalytic materials results in their poor performance, which restrains their applications. Thus, to enhance the photodegradation property of semiconducting PCs, it is necessary to suppress the recombination of charge carriers. In addition, using the conventional metal doping and addition of surfactants, carbon-based semiconductor hybrid materials have emerged as a new era of PCs, which has attracted significant attention recently.[286] Among the carbonaceous materials, graphene has received increasing attention due to its unique properties, such as high charge-carrier flexibility, high thermal and electrical conductivity, and extraordinary high surface area. These unique properties of graphene make it an ideal support material for semiconductor photocatalysts.

Furthermore, the interaction of graphene with semiconductor materials give rise to unique properties such as comprehensive light absorption and decreased charge carrier recombination rates, accompanied by high stability.[287] Therefore, graphene-semiconductor hybrid materials have been extensively used for the photodegradation of organic dyes, pharmaceutical drugs, antibiotics, organic phenolic compound, photocatalytic generation of hydrogen and disinfection. In this section, the main applications of graphene-assisted semiconducting photocatalysts such as NiO, TiO_2, Fe_3O_4, and ZnO are briefly summarized.

7.2. Photocatalytic degradation of dyes

Nowadays, a significant challenge is the inadequacy of pure and potable water, and its accessibility is becoming increasingly luxurious on a daily basis. This is due to the disposal of several toxic wastes from many industries, pharmaceutical laboratories and agricultural field. Among these effluents, inorganic and organic dyes are a major issue of concern. Thus, scientists are focusing on biodegrading dyes and dye-derived components. Biopolymers are the most preferable choice for the degradation of dyes due to their enhanced catalytic activities, as widely reported thus far. Millions of people in developing countries have been affected by diseases due to the unavailability of clean and pure drinking water and a safe hygienic environment. Thus, it is necessary to develop ecofriendly, cheap and easy processes to biodegrade these toxic dyes for the purification of water as the sources of portable water are vanishing daily and becoming ponds of eutrophicated, toxic, dirty and polluted water bodies. The major pollutants found in water bodies include pesticides, herbicides, dyes, and surfactants.[288] Thus, to overcome these problems, in the past few years, graphene-based photocatalysts have gained significant importance for photocatalytic applications. Due to their high photosensitivity, high surface area, excellent optical, mechanical and electrical properties, stability, eco-friendly and nontoxic nature, low cost and enhanced catalytic properties, they are being widely used in water cleansing and photodegradation of toxic dyes and chemical effluents.[289]

Rahimi *et al.* developed rGO/NiO nanowires for the photocatalytic disintegration of methyl orange (MO), which required both hydroxide and superoxide radicals.[248]

In another study, Elshypany *et al.*[249] described the solid-state-mediated magnetite zinc oxide (MZO) (Fe_3O_4/ZnO) with different ratios of rGO. The results revealed that the photodegradation activity of magnetite zinc graphene (MZG) was more than 98.5% against methylene blue. This was due to the synergistic effect of magnetite and zinc oxide in the presence of rGO.

Hamed *et al.*[250] reported the preparation of Gr/Pd/TiO_2 NPs and Gr/Pd/TiO_2 nanowalls *via* the combination of both hydrothermal and photo-deposition methods. They compared the degradation capacity of TiO_2 nanowalls, Gr/Pd/TiO_2 NPs and Gr/Pd/TiO_2-NWs towards Rhodamine B under UV light irradiation. The results showed that among them, the Gr/Pd/TiO_2 nanowalls had the best photodegradation activity owing to their high surface area.

Similarly, Zhang *et al.*[251] studied the photodegradation of MB in water by CuO–ZnO. Fe_2O_3/rGO and CuO–ZnO. Fe_2O_3/CNT. The degradation efficacy of the composite with CNT was better than rGO. Also, Chandra *et al.* demonstrated that graphene-Mn_2O_3 NCs showed almost 80% photodegradation activity against eosin, methylene blue, and rhodamine B.[252] Benjwal *et al.* explained the enriched photocatalytic degradation of MB dye *via* rGO-based TiO_2/Fe_3O_4 NCs with an efficiency of ~100% within 5 min.[253] Fu and co-workers synthesized magnetically separable graphene-based $ZnFe_2O_4$ PCs *via* a simple hydrothermal technique. The PCs revealed 88% degradation efficiency for MB, and further by adding H_2O_2 as a scavenging agent, the degradation activity was enhanced up to 99% at 90 min under visible light irradiation. It played a dual function as a photoelectron-chemical degrader and producer of hydroxyl radicals by the photo-electrochemical disintegration of H_2O_2.[254] Lv *et al.* reported the preparation of a ZnO-rGO composite *via* a rapid and simple microwave-assisted technique for the photocatalytic degradation of MB. In this study, rGO played a vital role in enhancing the photocatalytic activity. The results suggested that the ZnO-rGO NCs with 1.1 wt% of rGO achieved a supreme degradation efficacy of 88% in a neutral solution under UV light illumination compared to p-ZnO NPs (68%), which is attributed to the increased absorption property towards light absorption and large reduction in charge recombination.[255] Thangavel *et al.* demonstrated the photocatalytic behavior of synthesized β-$SnWO_4$-rGO NCs. The photodegradation efficiency of 55% and 60% was achieved by β-$SnWO_4$ NPs, whereas that of rGO-based NCs was found to be better at ~90 and 91% for methyl orange and Rhodamine B dyes, respectively.[256] Ag-Cu_2O ternary NCs reinforced by glucose-rGO with enhanced stability and visible light-induced photocatalytic action were proposed by Sharma *et al. via* a simple and green methodology at room temperature using glucose and Benedict's solution. The fabricated Ag-Cu_2O/rGO NCs showed excellent photocatalytic efficiency towards methyl orange dye, and their degradation rate was greater than the immaculate Cu_2O and Cu_2O/rGO NCs.[257] Isari *et al.* prepared ternary NCs of Fe-TiO_2 decorated on rGO *via* a simple sol–gel method. The DRS study of the fabricated PCs exhibited a tunable band gap, which introduces Fe ions into the titania structure. The maximum degradation efficiency for Rhodamine B was 91% in 120 min/sunlight using 0.6 g Fe-TiO_2/rGO NCs, with an initial pH of 6 in the photodegradation study.[258]

7.3. Degradation of antibiotics and pharmaceutical drugs

Besides adsorption, antibiotics can be efficiently decayed or decomposed into non-toxic small molecular species under different wavelengths of light (such as sunlight, visible and ultraviolet (UV) light) due to the presence of molecular active groups (*e.g.* superoxide ions (O_2) and hydroxyl radicals ($^{\bullet}OH$)) produced by photocatalysts.[249] Thus, the photocatalytic degradation technique is one of the most effective, operative, eco-friendly, and commonly used techniques for the degradation of antibiotic contaminants in the environment. Graphene, as an exciting material and encouraging PC, has been

broadly explored for the photodegradation of antibiotic toxins in water due to its high surface area for uniform distribution, tunable band-gap, exceptional electrical conductivity, fast electron transport, and cost-effective fabrication for large-scale production.[260] Generally, graphene-based photocatalysts are formed by adding other photocatalysts to overcome its disadvantages and improve its photocatalytic efficiency for degrading antibiotics. In the last few years, various efforts have been dedicated to developing and fabricating graphene-based semiconductor photocatalysts to increase the degradation capability of antibiotic pollutants. In this regard, Song *et al.* synthesized graphene/MnO_2 NCs *via* an *in situ* one-step hydrothermal route, which successfully degraded ~99.4% of the tetracycline residue in pharmaceutical wastewater.[261] In another study, Shanavas *et al.* studied the photodegradation capacity for tetracycline and ibuprofen drugs proficiently under visible light illumination in 90 min using Cu/$Bi_2Ti_2O_7$/rGO ternary NCs. The synthesized Cu/$Bi_2Ti_2O_7$/rGO PCs showed excellent charge carrier capture and the suppression of e^-–h^+ pair recombination, and the rGO sheets and Cu NPs also played an important role in the photocatalytic performances.[262] Lin *et al.* synthesized a TiO_2-reduced graphene oxide series with side-glowing optical fibers coating *via* the polymer-mediated hydrothermal deposition technique. The fabricated NCs displayed significantly superior photodegradation activities compared to the purely synthesized TiO_2. The utmost photocatalytic efficacy was perceived by 2.7% rGO, resulting in a degradation efficiency of about 54%, 81% and 92% for carbamazepine, ibuprofen, and sulfamethoxazole, respectively, under high-pressure UV illumination within 180 min, where the rate of mineralization of the pharmaceutical drugs was in the range of 52–59%.[263] Pastrana-Martínez *et al.* synthesized a modified TiO_2-GO composite *via* the liquid-phase deposition method for the degradation of diphenhydramine as a pharmaceutical drug, where the UV-visible light-assisted photodegradation of the drug was demonstrated. The modified TiO_2-GO composites demonstrated total degradation activity and substantial mineralization of diphenhydramine waste product in less than 60 min under UV/vis illumination for the optimum 3.3–4.0 wt%/GO in the modified TiO_2-GO composites. In another study, a family of cobalt NP-derived titania, functionalized by amine using graphene oxide as the base material was synthesized *via* the sol–gel and hydrothermal methods, revealing a remarkable degradation performance for oxytetracycline under both solar and visible light irradiation. The formation of a heterojunction between anatase phase titania and low concentration of Co_3O_4 NPs induced the photon-based oxidative degradation of oxytetracycline, and the addition of a small of amount GO enhanced its photodegradation activity. Amine-functionalized 2 wt% Co_3O_4/TiO_2/GO revealed exceptional rates and stability toward the degradation of oxytetracycline under visible light irradiation.[264] Similarly, Fe_3O_4/Mn_3O_4-rGO NCs were demonstrated to be an efficient photocatalyst for the photocatalytic degradation of an aqueous solution of sulfamethazine. The outcomes of the reaction shown 99% sulfamethazine photodegradation proficiency under the optimal conditions of 0.5 g L^{-1} concentration of Fe_3O_4/Mn_3O_4-rGO NCs, 0.07 mm L^{-1} sulfamethazine at pH 3 and temperature of 35 °C, and 6 mM concentration of H_2O_2.[265] Karthik *et al.* fabricated GO-decorated cerium molybdate nanocubes (Ce $(MoO_4)_2$/GO) for the photodegradation of chloramphenicol under visible light illumination. The (Ce$(MoO_4)_2$/GO) NCs exhibited an excellent photodegradation efficacy of towards chloramphenicol drug with the highest degradation efficiency of 99% within 50 min compared with pure Ce$(MoO_4)_2$ nanocubes. The remarkable photocatalytic performance of the NCs was attributed to the excellent charge separation of the photogenerated electrons and holes.[266]

7.4. Photocatalytic degradation of phenolic compounds

Fundamentally, organic dyes have been studied the most for the assessment of the photodegradation performance of graphene-based NCs.[290] Among the toxic organic pollutants found in industrial wastes, compounds such as phenol and phenolic compounds are essential to remove from water bodies.[291] The quantity of phenol in water must be retained at 0.1–1 mg L^{-1} (ppm) based on the environmental protection rules of the Pollution Control Board (1992). In this case, semiconductor PCs revealed enhanced photodegradation of phenol under stimulated solar/UV/visible irradiation after the integration of graphene.

Graphene-based TiO_2/ZnO NCs were prepared *via* a hydrothermal method by Malekshoar *et al.*,[267] and the photocatalytic profile of the coupled NCs with an optimized ratio was explored. The results revealed that the combined graphene-ZnO/TiO_2 NCs with a ZnO/TiO_2 to graphene ratio of 0.95 to 0.005 was superior compared to the single composite by a factor of 2. Furthermore, for the optimization of the reaction conditions, different parameters were investigated. The experimental investigation revealed that 1 h and graphene-ZnO/TiO_2 NCs were required for the degradation phenol (40 ppm) at neutral pH under solar irradiation of 100 mW cm^{-2}. The GO-TiO_2 NCs as a magnetic recyclable catalyst showed up to 99% degradation efficiency under UV irradiation within 60 min for carbamazepine and caffeine. Subsequently, the NCs were fully reusable and recoverable by magnetic separation. The additional advantages are that the GO-TiO_2 NCs were fully reusable, recoverable, and easy to fabricate.[268]

8. Electrochemical performances

Currently, the energy and environmental crises, such as the exhaustion of fossil fuels, environmental pollution and global are significant concerns in society. Thus, it is necessary to develop renewable energy storage and conversion materials, as well as the corresponding devices. In this framework, these problems can be overcome in two ways. Firstly, energy can be effectually converted from endless sources, mainly by the storage and conversion of electric and light energy to provide alternative energy sources to fossil fuels, *e.g.* the oxygen reduction reaction (ORR), water and solar power to relevant forms, such as electricity and fuel. To accomplish this goal,

Table 3 Summary of graphene-based metal oxide electrode materials

Graphene-based metal oxide	Name of electrolyte	Capacity (mA h g^{-1})/capacitance (F g^{-1})	Stability (%) (cycles)	Power/energy density
Fe_3O_4/rGO	1.0 M LiPF6 (EC : DMC, 1 : 1)	1000 mA h g^{-1}		
Graphene-$LiMn_2O_4$	1.0 M $LiPF_6$ (EC : DMC, 1 : 1)	130 mA h g^{-1}	87% (100)	
V_2O_3/rGO	1.0 M $LiPF_6$ (EC : DMC, 1 : 1)	823.4 mA h g^{-1}	89.9% (100)	4.0
SnO_2/rGO	1.0 M $LiPF_6$ (EC : DMC, 1 : 1)	1718 mA h g^{-1}	90.1% (50)	500
$ZnFe_3O_4$/GO/Chitosan	1.0 M H_2SO_4	830 F g^{-1}		650
rGO/ZnO	1 M Na_2SO_4	312 F g^{-1}	95.2% (1000)	
Graphene/$Ni_3V_2O_8$	2 M aq. KOH	748 F g^{-1}	71% (3000)	45.61
ZnO–CuO/N-rGO	1 M aq. KOH	1075 F g^{-1}	88% (5000)	1601
SnO_2/Co_3O_4/rGO	1 M H_2SO_4	317.2 F g^{-1}		1.2
NiO@$NiMoO_4$@PPy	1 M aq. KOH	941.6 F g^{-1}	77.1% (30 000)	
TrGO/Ni	1 M KOH	154.3 mA h g^{-1}	90.2% (2000)	
H-GTN	0.5 M BMIM-BF_4 50/CH_3CN	530 F g^{-1}	90.2% (100)	
Co–Ni/LDH nanosheets		3130.8 F g^{-1}	72.4% (3000)	
rGO@Fe_3O_4	1 M KOH	771.3 F g^{-1}	95.1% (5000)	
ZnOL@MpEG	1 M Na_2SO_4	347 F g^{-1}		5.0

fuel cells, solar cells and water splitting catalysts are required. Secondly, ecological benignity, cheap, and high performance are required by energy storage devices. This is essential because of the sporadic features of most renewable energy sources. Lithium-based batteries, including lithium ion, lithium–air and lithium–sulphur, are the most handy and capable devices for the storage of energy. Another encouraging and competent type device for energy storage is supercapacitors, which can store and release energy within a few seconds.[292] In the fields of catalysis and energy storage, the replacement of precious and rare metal electrodes and catalysts with commercially available substitutes has attracted much consideration from both industrial and academic researchers. However, although numerous studies have been performed, including the development of non-precious metal electrodes and catalysts, the results lag far behind the practical values due to the inadequate performance of the discovered materials and environmental hazards. It is worth noting that both theoretical calculations and experimental values have demonstrated the considerable activity of low-cost metal-free materials with unique electronic and nanostructures properties in a wide range of heterogeneous, electrochemical and catalytic processes.

Graphene, a material with outstanding properties, has gained popularity worldwide due to its applicability in an extensive range of applications, predominantly in the energy area. With the rapidly increasing population, an extreme necessity has arisen to explore alternative ways to meet the expanded energy demand, where the sources of non-renewable energy are limited. Especially, graphene-based metallic bimetallic and metal oxide NCs and graphene-based materials have gained immense popularity in the field of electrochemical energy storage. Because of their physico-chemical properties such as high thermal and chemical stability, large specific active surface area, excellent electrical conductive capability, good capacitance, and superior thermal and mechanical properties, graphene-based materials have been exploited as electrode materials in electrical energy storage devices.[293] Moreover, their broad potential range and rich surface chemistry have allowed the properties of storage devices to be customized.[294] Therefore, graphene-based metal oxides and polymer NCs have found wide applications in energy storage and energy conversion devices, such as batteries, supercapacitors, fuel and solar cells.[295–297] In this feature review article, we mainly focus on the electrochemical properties of graphene and its application towards lithium-based ion batteries, supercapacitors and ORR for fuel cells (Table 3).

8.1. Lithium-ion batteries (LIBs)

The ever-increasing requirement for advanced energy-density storage devices for power storage (power levelling) and transportation (electric-vehicles) is exciting for the scientific community to develop rechargeable batteries with a cycling performance comparable to that of Li-ion batteries but with significantly higher capacity. Carbon-constructed rechargeable batteries have attracted wide broad attention, specifically after the commercialization of Li-ion batteries by Sony laboratories, where metallic Li-ion is substituted by a carbon host structure, whereas the lithium ions can be absorbed and released reversibly at low electrochemical potentials. LIBs are considering encouraging candidates for the effective storage of energy owing to their high energy density and extensive life cycle. Their high definite capacity, enormous power density, and extended cyclic life are capable power cradles for electric vehicles. Although LIBs are the dominant power sources, their cathode and anode materials limit their energy density due to their nature and different characteristics. The most common configuration of LIBs is composed of an intercalated Li compound cathode (*e.g.*, $LiCoO_2$ and $LiFePO_4$), with a graphitic anode and corresponding organic carbonate electrolyte, with the graphitic anode attaining the highest energy densities id around 120–150 W h kg^{-1}.

At present, LIB technology is limited by the low theoretical specific capability of the standard graphite anodes as (372 mA h g^{-1}). Thus, the present research is focused on

developing alternative anode materials, for example Si (4200 mA h g^{-1}), Sn (994 mA h g^{-1}), and SnO_2 (782 mA h g^{-1}).

In the last two decades, due to the huge 'surface to mass ratio' beyond 2600 m^2 g^{-1}, with tremendous electrical conductivity and high and mechanical power with the extra value of large-scale production of graphene, it has emerged as an exciting anode material for LIBs. As a single layer, graphene has an inadequate competency to absorb Li-ions (surface coverage of 5%) due to the revulsion forces within the Li^+ ions at each side of the graphene layer, and thus significant work has been devoted to the exploitation of chemically modified graphene such as (GO) and (RGO), both at the anode and cathode positions. Graphene has also been used to anchor electrochemically energetic transition metal oxides, sulfides, nitrides, phosphides, and elements with alloying/dealloying mechanisms, for instance semiconductors, metals, and others.[296] Additionally, polymer electrolyte membranes (PEMs) are used for energy conversion and storage devices as an electrolyte or separator, which are essential components. PEMs play an important role in the devices prepared using functional polymers. Various PEMs comprised of several fillers have been established to accomplish the requirements of energy devices. Also, graphene-based NC anode materials have been synthesized for Li-ion batteries with enhanced performances. The enhancement in electrochemical performance of graphene-based NCs can be attributed to three aspects, as follows: (i) graphene layers possess flexibility, which suppresses the bulk expansion of these electrochemically energetic materials during the continuous process of charging/discharging and improves the accumulation/liquidation problems; (ii) the exceptional electrical conductivity of graphene ensures notable electrical interaction between neighboring heterogeneous particles. As discussed previously, graphene has a large-surface area, surface deficiencies and high porosity, giving rise to high Li storage capability, enhanced electrolyte accessibility and rapid Li-ion diffusion. Finally, (iii) confining electrochemically active NPs between graphene layers can mitigate the restacking of the graphene sheets layers, and subsequently retain their large surface area activity. These synergistic effects of both graphene sheets and NPs can combine the best qualities of both materials.

Tarascon's group reported the first study on metal oxides as anode materials with high capacity. Although metal oxides generally exhibit poor conductivity, properly tailored metal oxides on the nanoscale have demonstrated promising characteristics. The reaction mechanism of lithiation and delithiation in metal oxides can be generally classified into three main types (Fig. 16), as follows: (1) insertion/extraction, (2) alloying/dealloying, and (3) conversion mechanisms. The first mechanism is observed in different types of anode materials, MO_x (including anatase TiO_2). In fact, most cathode materials with layered or spinel structures also follow the insertion–extraction mechanism, as discussed previously. Alloy reactions exist in some main-group elements, including Si, Sb, Ge, Bi and Sn, which can alloy with lithium, forming Li_xM and providing a high specific capacity. However, the lithium alloying and dealloying processes are typically associated with huge

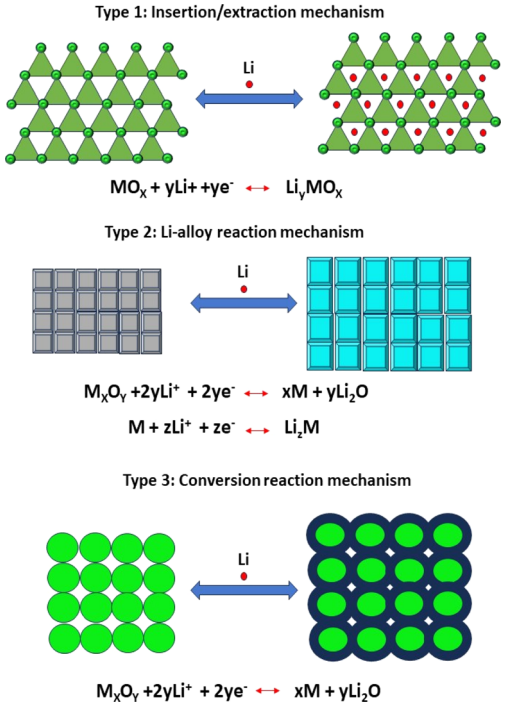

Fig. 16 Schematic of different mechanisms of reversible lithium-ion storage in metal oxides.

volumetric expansion (as high as 300%) and shrinkage, or pulverization, leading to capacity fading upon cycling. The third mechanism of conversion is typically observed in transition metal oxides (M_xO_y, M = Mn, Fe, Co, Ni, Cu, *etc.*). These conversion-type materials have relatively high theoretical capacities because they can incorporate more than one Li per metal. Metal grains and Li_2O are formed during the process of lithiation. In many cases, the metals can reversibly alloy with lithium. Metal oxides also have the issue of pulverization, huge first-cycle irreversible capacity loss, as well as poor conductivity. Thus, to overcome these problems, much effort has been focused on the preparation of nanoscale metal oxides and M_xO_y/carbon composites.[297–299]

The three types electrochemical reactions are as follows:

(1) Insertion reaction mechanism:

$$MO_x + yLi^+ + ye^- \leftrightarrow Li_yMO_x \quad (1)$$

(2) Li-alloy reaction mechanism:

$$M_xO_y + 2yLi^+ + 2ye^- \rightarrow xM + yLi_2O\ (e.g., SnO_2) \quad (2)$$

$$M + zLi^+ + ze - \leftrightarrow Li_zM \quad (3)$$

(3) Conversion reaction mechanism:

$$M_xO_y + 2yLi^+ + 2ye^- \leftrightarrow xM + yLi_2O \quad (4)$$

8.1.1. Graphene-based metal oxide NCs-based anodes. Staffolani *et al.* synthesized Fe_3O_4/rGO *via* co-precipitation and

high reduction temperature processes.[269,270] The as-synthesized material was composed of Fe_3O_4 NPs with a regular particle size, which were uniformly deposited on the rGO surface, showing a reversible capacity 2.5 times that of graphite and improved reversible capacity of $\approx$200 mA h g^{-1} at a rate of 10C (9260 mA g^{-1}). The anode materials were obtained by mixing the nanocomposites with Super C65 as a conducting agent and PAA as a binder in the ratio of 80 : 10 : 10, respectively, in an argon-filled glove box. Most significantly, the full cells assembled using these novel nanostructures as anodes and $LiNi_{1/3}Mn_{1/3}Co_{1/3}O_2$ as cathodes exhibited excellent capacity retention at various current rates. In another study, Kumar *et al.*[271] developed a 2D GO sheet enveloping 1D $LiMn_2O_4$ as NCs. The working lithium ion battery electrode was prepared with 80% active material, 10% super phosphorus and 10% polyvinylidene fluoride on Al foil. The NCs 3D porous cathode showed a high specific charge capacity of 130 mA h g^{-1} at a rate of 0.05C and coulombic efficiency of ~98% after 100 cycles in the potential window of 3.5–4.3 V *vs.* Li/Li^+ with encouraging initial charge capacity retention of ~87%, and exceptional structural stability even after 100 cycles, giving rise to a promising cathode NCs. Xiao *et al.*[272] successfully fabricated (V_2O_3/rGO) NCs *via* a simplistic solvothermal method and annealing process. In this synthesis protocol, V_2O_3 NPs were encapsulated by rGO. A coin-type cell (CR2025) was used in the electrochemical measurement. A LAND battery cycler was used to analyze the charge–discharge and cyclic performances of the cells over the potential range cs. Li/Li^+ at 25 °C. The Li^+ ion storage behaviour of V_2O_3/rGO was explored in the potential range of 0.01–3.0 V. The V_2O_3/rGO NCs achieved a high reversible specific capacity of 823.4 mA h g^{-1} under the current density of 0.1 A g^{-1}, and 407.3 mA h g^{-1} under the high current density of 4.0 A g^{-1}. Naresh *et al.* prepared SnO_2/rGO NCs *via* a microwave-mediated hydrothermal technique. The Li-ion batteries fabricated using pure globular-shape SnO_2 NPs and crumpled nanosheet-like morphology of SnO_2/rGO NCs, which acted as the anode material, exhibited the good initial discharge–charge capacity of 2128 and 1718 mA h g^{-1}, respectively. The capacity retention after 50 cycles was found to be 349 mA h g^{-1} at a current density of 500 mA g^{-1} for the Li-ion battery fabricated using pure globular-shape SnO_2 NPs and its capacity retention after 300 cycles was found to be 318 mA h g^{-1} at a current density of 500 mA g^{-1} for the Li-ion battery fabricated using SnO_2/rGO NCs, which was much better than the reported values.[273] A modified glassy carbon electrode (GCE) was prepared by mixing the synthesized NMs with carbon black and PVDF in the weight percentage of 80 : 10 : 10, respectively, using NMP solvent and grinding in a mortar. Alternatively, for the pure NPs, a 70 : 20 : 10 weight percentage was used. Lithium metal was used as the reference electrode, polypropylene (Celgard 2400) used as the separator and a mixture of 1 M $LiPF_6$ in ethylene carbonate (EC) and dimethyl carbonate (DMC) (1 : 1) as the electrolyte for the fabrication of Swagelok-type lithium-ion cells. The CV and GCD capacities of the fabricated Swagelok-type lithium-ion cells were recorded using a BCS 810 potentiostat (Biologic Instrument).

8.2. Supercapacitors

Supercapacitors are new higher energy storage devices with exclusive features such as high capacitance, high-power density, and very long cycle life, which are also called ultracapacitors/electrochemical capacitors. Supercapacitors have become a research hotspot among the new energy storage devices due to their unique characteristics of rapid charge–discharge rate, high-power density, long-term cycling stability, eco-friendly nature, light weight, low cost, flexibility, and high competence, which remain a challenging task in research. Ultracapacitors working based on electrochemical double layer capacitance (EDLC) are electrical energy storage devices storing and releasing energy by nanoscopic charge separation at the electrochemical interface between the electrode and electrolyte. In EDLC, energy is deposited through polarization, followed by the adsorption of ionic charges on the surface of the electrode, and hence the surface area of the electrode plays a significant role.[300] Because of their high specific surface area, porous nature, chemical inertness, and good electrical conductivity, carbon-based electrodes are promising for the fabrication of high-performance supercapacitors.[301] In contrast, graphene-based conducting polymers and metal oxides are favorable candidates for pseudocapacitance because of their electrochemically active nature and ability to carry out the faradaic redox reactions.[302] Low voltage spaces are the main obstacle for carbon-based materials to fully exploit their large surface area to accrue maximum charge and show greater capacitance. Organic electrolytes have been applied to increase the operational voltage windows instead of aqueous electrolytes, but their low thermal stability causes capacity fading. In this regard, ionic electrolytes have shown exciting results with large organic ions, low vapor pressure, wide liquid range, thermal stability, good electrochemical, and high ionic conductivity, together with extensive potential windows (typically, between 3 and 7 V).[303] Therefore, moisture adversely affects the performance of ionic electrolytes, and thus a highly sophisticated vapor-controlled process is required to utilize ionic electrolytes. However, this problem was successfully addressed by using hydrophobic ionic electrolytes. To improve the capacitance performance of carbon-based materials, scientists have employed different morphologies, *e.g.* wrinkled and 3D networks, and composites of various carbonaceous materials such as graphene/CNT and polymers.[304]

Presently, three types of pseudocapacitive mechanisms are known, as follows: (i) underpotential deposition, (ii) redox pseudocapacitance, and (iii) intercalation pseudocapacitance. Underpotential deposition occurs when the one metal ion forms an adsorbed monolayer on the surface of another metal with a higher redox potential. One of the classical examples is lead ions stacked on the surface of a gold electrode (Fig. 17a).

$$Au + xPb^{2+} + 2xe^- \leftrightarrow Au \cdot xPb_{ads}$$

Redox pseudocapacitance the most predominant pseudocapacitive reaction that appears when ions are electrochemically engaged or adsorbed on the surface or near-surface of materials together with faradaic charge transfer (Fig. 18b). These two

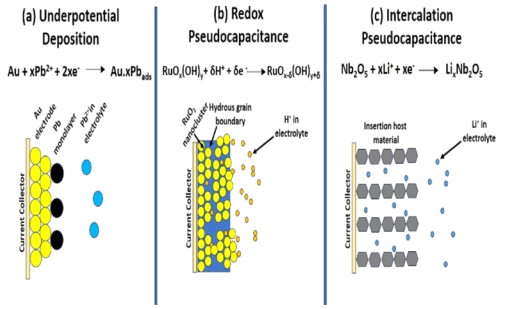

Fig. 17 Different types of reversible redox mechanisms that give rise to pseudocapacitance: (a) underpotential deposition, (b) redox pseudocapacitance, and (c) intercalation pseudocapacitance.

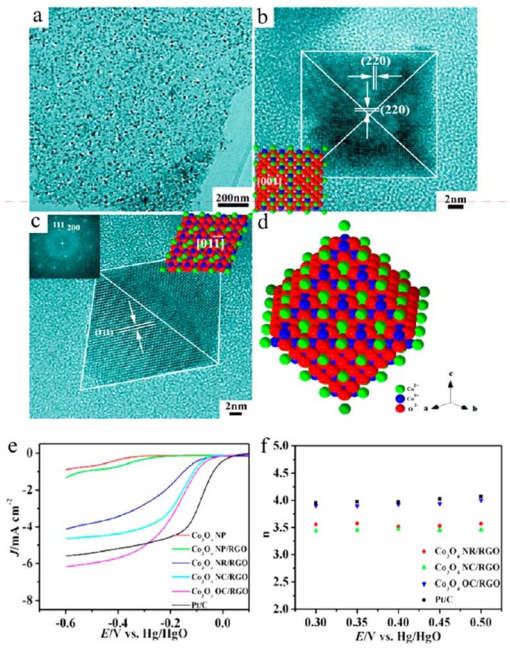

Fig. 18 (a) Low- and (b and c) high-resolution TEM images of Co_3O_4 nano-octahedron (OC) supported on the rGO sheet, with (d) schematic image of Co_3O_4 OC bounded by eight {111} surfaces. (e) Rotating-disk voltammograms of the Co_3O_4/rGO electrocatalysts made of Co_3O_4 and (f) electron transfer number deduced from the Koutecky–Levich equation. Reproduced with permission from ref. 281. Copyright 2013, Springer-Nature.

categories of pseudocapacitance are commonly applied in aqueous systems, which lead to a narrow potential window and limited energy density.

Herein, we discuss a representative structure (Fig. 17b), *i.e.*, RuO_2' xH_2O nanocluster arrayed electrode, for this application. In this scheme, the crystalline RuO_2' xH_2O nanotubes (NTs) (and the RuO_2' xH_2O underlayer) with metallic conductivity provide electron "superhighways" for charge storage and delivery. The arrayed, porous architecture of the RuO_2' xH_2O NTs substantially reduces the resistance to electrolyte penetration/diffusion.[305] Moreover, the hydrous nature of RuO_2' xH_2O promotes the rate of proton exchange (very different from the anodic aluminum oxide-based, anhydrous RuO_2 nanotubes prepared by means of thermal decomposition) given that the superficial redox transitions of RuO_2 involve a proton and electron double injecting/expelling process, which can be expressed as follows:

$$RuO_a{\cdot}(OH)_b + \delta_H{}^+ + \delta e^- \leftrightarrow RuO_{a-\delta}(OH)_{b+\delta}$$

Intercalation pseudocapacitance with a charge storage process takes place in the bulk material, exhibiting different electrochemical features from redox pseudocapacitance and underpotential deposition in a non-aqueous electrolyte system.

Conway previously suggested that this intercalation process is an intermediate behaviour between batteries and supercapacitors, where Li^+ ions are actually accommodated in quasi-two-dimensional planes in the van der Waals gap of the host lattice material (Fig. 17c).

The proposed energy storage mechanism of "intercalation pseudocapacitance" has enormously expanded the research field of pseudocapacitive materials. The first to be uncovered was the pseudocapacitive mechanism of lithium-ion insertion into many polymorphic forms, such as pseudohexagonal (TT-Nb_2O_5), orthorhombic (T-Nb_2O_5), tetragonal (M-Nb_2O_5), and monoclinic phases (H-N Nb_2O_5). Amongst them, T-Nb_2O_5 is an orthorhombic phase crystal, which has been proven to be the most potential candidate for intercalation-type pseudocapacitive energy storage.[306] T-Nb_2O_5 is mainly composed of highly distorted octahedral and pentagonal bipyramidal Nb environments. Its unit cell has sheets of edge- or corner-sharing distorted polyhedra lying parallel to the (001) plane, with each Nb^{5+} surrounded by either 6 or 7O^{2-}. The mainly empty octahedral sites between the (001) planes offer suitable tunnels for Li^+ transport throughout the ab plane. Charge storage from the intercalation of Li^+ into Nb_2O_5 can be indicated as follows:

$$Nb_2O_5 + xLi^+ + xe^- \leftrightarrow Li_xNb_2O_5\ (0 \le x \le 2)$$

Suneetha *et al.* prepared zinc-doped iron oxide/graphene oxide/chitosan NCs using an optimized quantity of constituents *via* a simple solution casting method. The bandgap was calculated to be 2.28 eV, which specifies the conducting nature of the composite. The formation of the composite in nano dimensions of around 20 nm was proven by XRD, SEM and HRTEM studies. The electrochemical profile of the composite was examined by cyclic voltammetry and capacitive performance by impedance studies (EIS). Three electrodes were used for the measurement cyclic voltammetry. The working electrode was made by coating a glassy carbon with the NCs, while 1.0 M sulphuric acid-containing NCs were casted on GC as the working electrode. The electrochemical studies showed the good adherent nature of the composite on the electrode surface at pH 1 and greater electrochemical stability with well-defined redox peaks. EIS showed that the NC-modified electrode revealed a good capacitance performance with a Bode phase angle of 87°, which verifies that it is a good candidate for supercapacitor applications.[274,275] Jayachandrian *et al.*[276] fabricated ZnO and rGO/ZnO NCs as

electrode materials for application in supercapacitors. A straightforward and economical technique was used for the fabrication of rGO/ZnO NCs *via* ultrasonication. The electrode was prepared with 80 wt% of active material, 10 wt% of acetylene black and 10 wt% of PVDF mixed using NMP solvent and grinding in a mortar. The prepared electrode was examined with the help of by cyclic voltammetry, chromo-potentiometry (CP), cycling stability and electrochemical impendence spectroscopy (EIS). The electrochemical performance of rGO/ZnO NCs displayed that the synthesized composite has a strong specific capacitance (312 F g^{-1}) in comparison with pure ZnO NPs (200 F g^{-1}) with improved cycling stability up to 1000 cycles. Low *et al.*[277] synthesized graphene/$Ni_3V_2O_8$ NCs *via* the solvothermal method as a facile approach. Liquid-phase exfoliation is an ecofriendly approach for the fabrication of graphene sheets with the optimized volume ratio of ethanol to water (2 : 3). The electrochemical properties and the integrated advantages of the graphene sheet and pseudocapacitive nature of $Ni_3V_2O_8$ resulted in a superior electrochemical performance to the pristine $Ni_3V_2O_8$, demonstrating that it is a promising material. The working electrode was prepared with PVDF as the binder and carbon black as the conducting agent in the presence of NMP solvent, while 2 M KOH was used as the electrolyte for application in Li-ion batteries. CV and EIS were performed on an electrochemical workstation, and the GCD and cyclic stability test were carried on an Arbin instruments (BT-2000) using G 4NVO (graphene/$Ni_3V_2O_8$ with the weight ratio of 1 : 4). The nanocomposite delivered the high specific capacitance of 748 F g^1 at a current density of 0.5 Ag^{-1}, remarkable energy density of 103.94 W h kg^{-1} at a power density of 45.61 kW kg^{-1}, reasonable cycling stability with 71% capacitance retention and superior coulombic efficiency of 83% after 3000 charge–discharge cycles at 0.5 Ag^{-1}. Maity *et al.*[278] fabricated plate-like CuO and flower-like ZnO anchored on rGO and nitrogen-doped rGO following a simple large-scale production, economical, facile hydrothermal technique. XRD, FTIR and XPS studies authenticated the presence of the N-doped material on rGO sheets in all the synthesized composites. The electrochemical performance of all the composites was investigated by CV, GCD and EIS in a three-electrode configuration using 1 M aqueous KOH, platinum foil as the counter and Ag/AgCl as the reference electrode. The electroactive materials, dispersed in ethanol and mixed with 0.5% Nafion as binder, were mounted on a pre-acid-treated graphite rod (working electrode). They observed the high energy density (ED) value of the synthesized NCs to be 95.55 W h kg^{-1} with a power density (PD) of 399.97 W kg^{-1}. The electrode made up of hybrid ZnO–CuO/N-rGO NCs revealed admirable cyclic stability of 88% specific capacitance retention after 5000 cycles. In another study, Nagarani *et al.*[279] fabricated SnO_2/Co_3O_4/rGO NCs *via* the conventional technique to estimate their enhanced electrochemical properties for supercapacitor applications. The modified glassy carbon electrode (GCE) was prepared by mixing the synthesized NMs with carbon black and PVDF in a weight percentage of 80 : 10 : 10, respectively. The electrochemical properties of the modified electrode were investigated in a standard three-electrode cell, which also included a platinum electrode (counter) and Ag/AgCl (reference electrode). The electrochemical properties of the composites were studied be performing CV, GCD and EIS on an electrochemical workstation. BTMO/rGO NCs with a modified surface to volume ratio and enhanced electron conductivity were observed to have an enlarged integral area and current of 2.5117×10^{-4} A s^{-1} and 3.1686×10^{-4} A, respectively, in CV. The NCs also showed an increased specific capacitance value of 317.2 F g^{-1} at 1 A g^{-1}. The increased specific capacitance value of BTMO/rGO NCs was largely due to the synergistic effect between SnO_2/Co_3O_4 and rGO.

8.3. Oxygen reduction reaction for fuel cells

Fuel cells are energy conversion devices, where chemical energy is converted to electrical energy using oxidizing fuel catalyzed by different catalysts, which are restrained on the electrodes. Fuel cells produce electricity by reactions occurring between the fuel at the anode and oxidant at the cathode, which are uninterruptedly delivered from external sources. Fuel cells have huge potential as clean and competent power sources for EVs because of their high energy translation efficiency, low operation temperature, low or zero emission, high energy and power density. However, the slow kinetics of the ORR ($O_2 + 4H^+ + 4e/2H_2O$) is the main aspect limiting the energy conversion competence of fuel cells and their large-scale commercialization. Hence, developing capable electrocatalysts for the OR reaction at the cathode in fuel cells is necessary.[307] In a fuel cell, polymer electrolyte membrane fuel cells (PEMFC) are considered exciting materials for electrochemical devices owing to their high power density and low greenhouse gas emissions.[308] Among the numerous types of fuel cells, low-temperature PEMFCs have been widely investigated due to their extraordinary features such as high competence and speedy start-up.[42] Graphene and its derivatives are of particular interest in PEMFCs.[45–47] Among the oxidized forms of graphene, graphene oxide has been regularly used.[309] However, pure graphene oxide is an electronic insulator with a differential conductivity in the range of 1 to 5×10^{-3} Scm^{-1} at a bias voltage of 10 V.[310]

Wu *et al.* synthesized an N-doped rGO anchored Fe_3O_4 NP aerogel with enriched ORR activity compared to N-doped carbon soot and N-doped graphene sheets and sustained a close to 4-electron transfer even at a low voltage.[280] To gain insight into the ORR activity of the Fe_3O_4 NPs supported on the 3D macroporous N-GAs, the electrocatalytic properties of Fe_3O_4/N-Gas were investigated in N_2- and O_2-saturated 0.1 M aqueous KOH electrolyte solution using cyclic voltammetry at a scan rate of 100 mV s^{-1}. The restrained Fe_3O_4 NPs within the graphene layers were thought to enrich the interfacial charge transfer contact between the metal oxide and the graphene sheet, while protecting the NPs against dissolution and agglomeration. A similar structure of CoO on N-doped rGO showed excellent durability compared to Pt/C. By synthesizing Co_3O_4 nanocubes (NC), nanorods (NR), and nano-octahedra (OC) on rGO, where each shape was defined by different facets, Xiao *et al.*[281] established that the ORR activity follows the sequence {111} > {100} ≫ {110} (Fig. 18). This demonstrated

the surface structure-dependent electrocatalytic activity of Co_3O_4 NPs anchored on graphene sheets toward the oxygen reduction reaction. The ORR kinetics of the Co_3O_4/rGO composites was investigated using the rotating-disk electrode (RDE) technique in O_2-saturated 0.1 M KOH electrolyte. Similarly, flower-shaped MnO_2 NPs decorated on rGO showed great selectivity toward four-electron reduction and high tolerance toward methanol. By replacing Co^{3+} with Mn^{3+} in the spinel $MnCo_2O_4$/N-doped rGO, it was possible to achieve greater ORR activity than Pt/C at a medium overpotential with high selectivity toward the 4-electron transfer reaction. Other spinel mixed oxide composites such as $NiCo_2O_4$/rGO and $CuCo_2O_4$/N-doped rGO NCs have shown huge potential in ORR in terms of methanol tolerance and high durability, respectively.[282]

9. Conclusion, future perspectives and challenges

This review article presented the most recent literature with a focus on the recent research progress in graphene and graphene-based metal oxide NCs. Initially, we discussed various eco-friendly methods for the synthesis of GO and rGO sheets with, highlighting the latest available bottom-up approaches for the fabrication of bioinspired graphene/rGO using GO as an initiator. Thus, the precise control of surface defects and superficial-scale production of GO or rGO NSs are highly anticipated. Efforts should be devoted to the establishment of cost effective, eco-friendly, stable and recyclable NMs for large-scale application at the industrial level with significant electrochemical properties and photocatalytic performance. Furthermore, we discussed some of the most recently established advanced green methods for the large-scale synthesis of graphene-based metal oxide NCs, focusing on the conventional and bioinspired synthesis of graphene-based metal oxides NCs. Especially, the photosynthesis of graphene-based metal oxide NCs has emerged as a remarkably attractive methodology in the last decade. Numerous varieties of plant extracts (bio-constituents including plants, fungi, algae, bacteria, yeast and other plant-mediated extracts) have been considered as efficient resources for the synthesis/fabrication of several graphene-based materials. Among the aforementioned components, plant extracts were shown to exhibit supreme efficiency as reducing, stabilizing agent and capping agents for the controlled synthesis of materials, *i.e.*, shapes, sizes, structures, surface area, crystallinity and other specific features. The controlled synthesis of these NMs inhibits the restacking of the graphene NSs and provides awesome templates for the preparation of porous networks with improved electronic and electrical properties. This wide range of graphene nanohybrid structures such as metal oxide-encapsulated, sandwiched, anchored, wrapped, mixed and layered structures with graphene has been studied. Furthermore, graphene nanohybrids with various nano-architectures and particle size, pore size and shape, conductive nano-channels, 2D to 3D interconnected network structures, spongy framework, *etc.* have huge potential for many industrial applications in the field of catalysis and energy storage system have also been demonstrated.

Lastly, we concluded this review with inclusive descriptions of the applications of graphene-based NCs as semiconductor photocatalysts for the degradation of dyes, pharmaceutical drugs, antibiotics and phenolic compounds. In this photocatalytic study, graphene-based semiconductor photocatalysts, mechanistic properties, newest literature for considering the optimization parameters of the system such as photocatalyst dose, initial dye concentration, pH, temperature, light intensity, presence of oxidizing agents/electron acceptors and the presence of ionic compounds were examined accurately and the optimum degradation efficiency discussed. This review highlighted several morphologies connected with novel constructions based on NH materials, which greatly help in improving the electrochemical performance of graphene-based metal oxide NCs as electrodes with enhanced charge-storage capacity, increased rate capability, improved reliability of devices with cycling stability, and increased energy and power densities, galvanic charge discharge, pseudo-capacitance nature, and reaction mechanism of anode or electrode materials for LIBs and super-capacitors.

The major challenge in the synthesis of graphene and graphene-based NCs is their large-scale production, which needs tremendous efforts. The challenges are as follows: (i) how to prevent the accumulation of graphene in the matrix, (ii) how to regulate the surface defects in graphene; and (iii) how to enhance the desired application-based properties. There are different methodologies for the synthesis graphene. Although the green synthesis or reduction of graphene oxide is a cost-effective, environmentally friendly, and simple approach for the reduction of graphene oxide, it results in poor conductivity or defects in the graphene sheets, which are also major challenges in the large-scale production of reduced graphene oxide using phytoextracts. In case of energy devices, security is a main attention in anode design for viable batteries. Actual battery conditions are often more complicated than laboratory experimental conditions. The mechanical stability and safety of the battery cannot be overlooked. Instantaneously, the selection of materials for the production of battery electrode materials should avoid noxious and destructive substances. The use of eco-friendly or non-hazardous complexes and composites should be preferred, not only to protect consumers but also to reduce the risk to the surroundings, which is noble for reprocessing.

Author contributions

Conceptualization: A. K. P., S. K. T. A., M. M. A., S. R. W. and R. G. C.; visualization: A. K. P., S. K. T. A., A. S. K., R. S. M., and A. D.; supervision: S. H. W., S. H. M., A. A. A., R. A, and R. G. C.; writing–original draft: A. K. P., S. K. T. A., M. M. A., A. K., R. M., and R. G. C.; writing, reviewing & editing: A. D., A. A. A., S. H. M., R. A., and R. G. C.

Consent for publication

All the consent has been reproduced from the publisher with permission for publishing the data.

Conflicts of interest

The authors declare no conflict of interest, financial or otherwise.

Acknowledgements

The authors are grateful to Principal, Seth Kesarimal Porwal College of Arts and Science and Commerce, Kamptee, for providing journal access facility. Moreover, we are heartily thankful to RGC, SHM and RA for their valuable inputs and continuous inspiration to write a review article.

Notes and references

1 C. E. E. Rao, A. E. Sood, K. E. Subrahmanyam and A. Govindaraj, *Angew. Chem., Int. Ed.*, 2009, **48**(42), 7752–7777.
2 I. Langmuir, *J. Am. Chem. Soc.*, 1918, **40**, 1361–1403.
3 K. S. Novoselov, A. K. Geim, S. V. Morozov, D. Jiang, Y. Zhang, S. V. Dubonos, I. V. Grigorieva and A. A. Firsov, *Science*, 2004, **306**, 666–669.
4 C. Lee, X. Wei, J. W. Kysar and J. Hone, *Science*, 2008, **321**, 385–388.
5 A. Balandin, S. Ghosh, W. Bao, I. Calizo, D. Teweldebrhan, F. Miao and C. Lau, *Nano Lett.*, 2008, **8**, 902–907.
6 A. Castro Neto, F. Guinea, N. Peres, K. Novoselov and A. Geim, *Rev. Mod. Phys.*, 2009, **81**, 109–162.
7 J. U. Lee, D. Yoon and H. Cheong, *Nano Lett.*, 2012, **12**, 4444–4448.
8 C. Xu, B. Xu and Y. Gu, *Energy Environ. Sci.*, 2013, **6**, 1388–1414.
9 A. K. Potbhare, R. Bagade, P. B. Chouke, S. Zahra, T. Lambat, M. B. Bagade and R. G. Chaudhary, *Mater. Today: Proc.*, 2019, **15**, 454–463.
10 A. Swain, L. Pradhan and D. Bahadur, *ACS Appl. Mater. Interfaces*, 2015, **7**, 8013–8022.
11 S. Mukherjee, X. Meshik, M. Choi, S. Farid, D. Datta, Y. Lan, S. Poduri, K. Sarkar, U. Baterdene, C. E. Huang, Y. Y. Wang, P. Burke, M. Dutta and M. A. Stroscio, *IEEE Trans. NanoBiosci.*, 2015, **14**, 967–972.
12 V. N. Sonkusare, R. G. Chaudhary, G. S. Bhusari, A. Mondal, A. K. Potbhare, R. K. Mishra, H. D. Juneja and A. Abdala, *ACS Omega*, 2020, **5**, 7823–7835.
13 X. Hu, G. Wang, B. Wang, X. Liu and H. Wang, *Chem. Eng. J.*, 2019, **355**, 986–998.
14 C. Liao and S. Wu, *Chem. Eng. J.*, 2019, **355**, 805–814.
15 H. Y. Hafeez, S. K. Lakhera, P. Karthik, M. Anpo and B. Neppolian, *Appl. Surf. Sci.*, 2018, **449**, 772–779.
16 C. Tian, L. Wang, F. Luan and X. Zhuang, *Talanta*, 2019, **191**, 103–108.
17 M. Puiu and C. Bala, *Bioelectrochem*, 2018, **120**, 66–75.
18 A. K. Potbhare, P. B. Chouke, A. Mondal, R. Thakare, S. Mondal, R. G. Chaudhary and A. R. Rai, *Mater. Today: Proc.*, 2020, **29**, 939–945.
19 M. Zhang, C. Liao, Y. Yao, Z. Liu, F. Gong and F. Yan, *Adv. Funct. Mater.*, 2014, **24**, 978–985.
20 B. Zhang, C. Li, H. Zhang, Y. Chen, H. Jiang, L. Chen, F. Ur Rehman and X. Wang, *J. Biomed. Nanotechnol.*, 2018, **14**, 1277–1286.
21 P. J. Sephra, P. Baraneedharan, M. Sivakumar, T. D. Thangadurai and K. Nehru, *Mater. Res. Bull.*, 2018, **106**, 103–112.
22 S. Das, K. Sa, I. Alam and P. Mahanandia, *Mater. Lett.*, 2018, **232**, 232–236.
23 W. C. Dong, J. C. Hyun, F. Alan and B. B. Jong, *J. Mater. Chem.*, 2014, **2**, 12136–12149.
24 P. P. A. Jose, M. S. Kala, N. Kalarikkal and S. Thomas, *Res. Chem. Intermed.*, 2018, **44**, 5597–5621.
25 D. Xu, B. Cheng, W. Wang, C. Jiang and J. Yu, *Angew. Chem., Int. Ed.*, 2018, **231**, 368–380.
26 S. Qu, Y. Xiong and J. Zhang, *Sep. Purif. Technol.*, 2019, **210**, 382–389.
27 T. Chen, Y. Zhou, J. Zhang and Y. Cao, *Int. J. Electrochem. Sci.*, 2018, **13**(9), 8575–8588.
28 F. Gao, C.-L. Yang, M.-S. Wang, X.-G. Ma and W.-W. Liu, *Spectrochim. Acta, Part A*, 2019, **206**, 216–223.
29 N. Yousef, X. Sun and X. Lin, *Adv. Mater.*, 2014, **26**, 5480–5487.
30 G. Lui, J. Y. Liao and A. Duan, *J. Mater. Chem. A*, 2013, **1**, 12255–12262.
31 B. Li and H. Cao, *J. Mater. Chem.*, 2011, **21**, 3346.
32 L. Zhu, Z. Liu, P. Xia, H. Li and Y. Xie, *Ceram. Int.*, 2018, **44**, 849–856.
33 S. Lathasree, A. N. Rao, B. SivaSankar, V. Sadasivam and K. Rengaraj, *J. Mol. Catal. A: Chem.*, 2004, **223**, 101.
34 C. Chen, J. Xi and E. Zhou, *Nano-Micro Lett.*, 2017, **10**, 26.
35 D. Wang, W. Yan, S. H. Vijapur and G. G. Botte, *Electrochim. Acta*, 2013, **89**, 732–736.
36 H. Chen, M. Müller, K. Gilmore, G. Wallace and D. Li, *Adv. Mater.*, 2008, **20**, 3557–3561.
37 V. C. Tung, M. J. Allen, Y. Yang and R. B. Kaner, *Nat. Nanotechnol.*, 2008, **4**, 25–29.
38 B. Jayasena and S. Subbiah, *Nanoscale Res. Lett.*, 2011, **6**(1), 95–101.
39 M. Yi and Z. Shen, *J. Mater. Chem.*, 2015, **3**, 11700–11715.
40 J. Kwak, S. Y. Kim, Y. Jo, N. Y. Kim, S. Y. Kim, Z. Lee and S. Y. Kwon, *Adv. Mater.*, 2018, **30**, 1800022.
41 M. Jin, H. Jeong, T. Kim, K. So, Y. Cui, W. Yu and J. Phy, *Appl. Phys.*, 2010, **43**, 275402.
42 C. Li, X. Wang, Y. Liu, W. Wang, J. Wynn and J. Gao, *J. Nanopart. Res.*, 2012, **14**, 1–11.
43 D. Parviz, F. Irin, S. A. Shah, S. Das, C. B. Sweeney and M. J. Green, *Adv. Mater.*, 2016, **28**, 8796–8818.
44 C. Chen, Z. Xu and Y. Han, *ACS Appl. Mater. Interfaces*, 2016, **8**, 8000–8007.
45 S. Pei, J. Zhao, J. Du, W. Ren and H.-M. Cheng, *Carbon*, 2010, **48**, 4466–4474.

46 G. Sun, X. Li, Y. Qu, X. Wang, H. Yan and Y. Zhang, *Mater. Lett.*, 2018, **62**, 703–760.
47 K. Subrahmanyam, L. Panchakarla, A. Govindaraj and C. Rao, *J. Phys. Chem. C*, 2009, **113**, 4257–4259.
48 I. Janowska, O. Ersen, T. Jacob, P. Vennégues, D. Bégin and M.-J. Ledoux, *Appl. Catal., A*, 2009, **371**, 2–30.
49 C. Wu, X. Huang and X. Wu, *Nanoscale*, 2013, **5**, 3847–3855.
50 M. Acik, G. Lee, C. Mattevi, A. Pirke, R. Wallace, M. Chhowalla, K. Cho and Y. Chabal, *J. Phys. Chem. C*, 2015, **115**, 19761–19781.
51 M. S. Umekar, G. S. Bhusari, A. K. Potbhare, A. Mondal, B. P. Kapgate, M. F. Desimone and R. G. Chaudhary, *Curr. Pharm. Biotechnol.*, 2021, **22**, 1759–1781.
52 A. H. Abdullah, Z. Ismail, A. S. Z. Abidin and K. Yusoh, *Mater. Chem. Phys.*, 2019, **222**, 11–19.
53 Z. Ismail, N. F. A. Kassim, A. H. Abdullah, A. S. Z. Abidin, F. S. Ismail and K. Yusoh, *Mater. Res. Express*, 2017, **4**, 075607.
54 O. Sadak, A. K. Sundramoorthy and S. Gunasekaran, *Carbon*, 2018, **31**, 108–117.
55 E. Secor, T. Gao, A. E. Islam, R. Rao, S. G. Wallace, J. Zhu, K. W. Putz, B. Maruyama and M. Hersam, *Chem. Mater.*, 2017, **19**, 2332–2340.
56 H. Akhavan-Zanjani, M. Saffar-Avval, M. Mansourkiaei, F. Sharif and M. Ahadi, *Int. J. Therm. Sci.*, 2016, **100**, 316–323.
57 W. Lv, D.-M. Tang, Y.-B. He, C.-H. You, Z.-Q. Shi and X.-C. Chen, *ACS Nano*, 2009, **3**, 3730–3736.
58 K. Q. Deng, J.-h. Zhou and X.-F. Li, *Colloids Surf., B*, 2013, **101**, 183–188.
59 M. A. Raj and S. A. John, *Anal. Chim. Acta*, 2013, **771**, 14–20.
60 X. Liu, H. Kim and L. J. Guo, *Org. Electron.*, 2013, **14**, 591–598.
61 O. Akhavan, *Carbon*, 2011, **29**, 11–18.
62 S. Toh, K. Loh, S. Kamarudin and W. Daud, *J. Chem. Eng.*, 2014, **251**, 422–434.
63 A. K. Potbhare, T. S. Shrirame, V. Devthade, S. T. Yerpude, M. S. Umekar, R. G. Chaudhary and G. S. Bhusari, *Biogenic Sustainable Nanotechnology: Trends and Progress*, Elsevier, 2022, pp. 149–184.
64 P. Marchezi, G. Sonai and M. Hirata, *J. Phys. Chem. C*, 2016, **120**, 23368–23376.
65 F. W. Low, C. W. Lai and S. B. A. Hamid, *Ceram. Int.*, 2015, **41**, 5798–5806.
66 D. Zhang, Y. Zhang and Y. Luo, *Nano Res.*, 2018, **11**, 1651–1663.
67 S. Thakur and N. Karak, *Carbon*, 2012, **50**, 5331–5339.
68 S. Stankovich, D. Dinkin, R. Piner, K. A. Kohlhaas, A. Kleinhammes, Y. Jia, Y. Wu, S. T. Nguyen and R. S. Ruoff, *Carbon*, 2007, **45**, 1558–1565.
69 N. Mahmood, C. Zhang, H. Yin and Y. Hou, *J. Mater. Chem. A*, 2014, **2**, 15–32.
70 F. Bonaccorso, L. Colombo, G. Yu, M. Stoller, V. Tozzini, A. C. Ferrari, R. S. Ruoff and V. Pellegrini, *Science*, 2015, **347**, 1246501–1246509.
71 W. Li, F. Wang, Y. Liu, J. Wang, J. Yang, L. Zhang, A. A. Elzatahry, D. Al-Dahyan, Y. Xia and D. Zhao, *Nano Lett.*, 2015, **15**, 2186–2193.
72 R. G. Chaudhary, G. S. Bhusari, A. D. Tiple, A. R. Rai, S. R. Somkuvar, A. K. Potbhare, T. L. Lambat, P. P. Ingle and A. A. Abdala, *Curr. Pharmaceut. Des.*, 2019, **25**, 4013–4029.
73 R. Bagade, V. Sonkusare, A. K. Potbhare and R. G. Chaudhary, *Mater. Today: Proc.*, 2020, **15**, 566–574.
74 S. Navalon, A. Dhakshinamoorthy, M. Alvaro and H. Garcia, *Chem. Rev.*, 2014, **114**, 6179–6212.
75 B. Luo and L. Zhi, *Energy Environ. Sci.*, 2015, **8**, 456–477.
76 S. K. Vashist and J. H. Luong, *Carbon*, 2015, **84**, 519–550.
77 A. Kamyshny and S. Magdassi, *Small*, 2014, **10**, 3515–3535.
78 K. Ullah, S. Ye, Z. Lei, K.-Y. Cho and W.-C. Oh, *Catal. Sci. Technol.*, 2015, **5**, 184–198.
79 M. Tang, X. Wang, F. Wu, Y. Liu, S. Zhang, X. Pang, X. Li and H. Qiu, *Carbon*, 2014, **71**, 238–248.
80 Y. Zhu, S. Murali, W. Cai, X. Li, J. W. Suk, J. R. Potts and R. S. Ruoff, *Adv. Mater.*, 2010, **22**, 3906–3924.
81 B. Xia, Y. Yan, X. Wang and X. W. D. Lou, *Mater. Horiz.*, 2014, **1**, 379–399.
82 C. Xu, X. Wang and J. Zhu, *J. Phys. Chem. C*, 2008, **112**, 19841–19845.
83 A. Bhirud, S. Sathaye, R. Waichal, J. Ambekar, C. Park and B. Kale, *Nanoscale*, 2015, **7**, 5023–5034.
84 J. Leng, W.-M. Wang, L.-M. Lu, L. Bai and X.-L. Qiu, *Nanoscale Res. Lett.*, 2014, **9**(99), 1–8.
85 S. Stankovich, D. A Dikin, G. H. Dommett, K. M. Kohlhaas, E. J. Zimney, E. A. Stach, R. Piner, S. T. Nguyen and R. S. Ruoff, *Nature*, 2006, **442**, 282–286.
86 S. F. Adil, M. Assal, M. Khan, A. Al-Warthan, M. R. H. Siddiqui and L. M. Liz-Marzań, *Dalton Trans.*, 2015, **44**, 9709–9717.
87 R. G. Chaudhary, A. K. Potbhare, P. B. Chouke, A. R Rai, R. K. Mishra, M. F Desimone and A. A. Abdala, *Applications of Emerging Nanomaterials and Nanotechnology, Material Research Foundations*, 2020, vol. 83, pp. 79–116.
88 P. B Chouke, A. K Potbhare, G. S Bhusari, S. Somkuwar, D. P. M. D. Shaik, R. K Mishra and R. G. Chaudhary, *Adv. Mater. Lett.*, 2018, **10**, 355–360.
89 J. Chen, B. Yao, C. Li and G. Shi, *Carbon*, 2013, **64**, 225–229.
90 M. N. Nadagouda and R. S. Varma, *Cryst. Growth Des.*, 2007, **7**, 2582–2587.
91 M. Bahram, F. Hoseinzadeh, K. Farhadi, M. Saadat, P. NajafiMoghaddam and A. Afkhami, *Colloids Surf., A*, 2014, **441**, 517–524.
92 N. I. Hulkoti and T. Taranath, *Colloids Surf., B*, 2014, **121**, 474–483.
93 M. S. Akhtar, J. Panwar and Y.-S. Yun, *ACS Sustain. Chem. Eng.*, 2013, **1**, 591–602.
94 A. K. Potbhare, R. G. Chaudhary, P. B. Chouke, S. Yerpude, A. Mondal, V. N. Sonkusare, A. R. Rai and H. D. Juneja, *Mater. Sci. Eng., C*, 2019, **99**, 783–793.
95 P. B. Chouke, A. K. Potbhare, N. P. Meshram, M. M. Rai, K. M. Dadure, K. Chaudhary, A. R. Rai, M. F. Desimone,

R. G. Chaudhary and D. T. Masram, *ACS Omega*, 2022, **7**(8), 6869–6884.
96 M. Umekar, R. Chaudhary, G. Bhusari and A. Potbhare, *Emerging Mater. Res.*, 2021, **10**, 75–84.
97 P. R. Bhilkar, R. S. Madankar, T. S. Shrirame, R. D. Utane, A. K. Potbhare, S. Yerpude, S. R. Thakare, A. A. Abdala and R. G. Chaudhary, *Emerging Nanomaterials and Their Impact on 21st Century, Materials Research Forum*, 2022, vol. 135, pp. 55–82.
98 N. B. Singh, R. G. Chaudhary, M. F. Desimone, A. Agrawal and S. K. Shukla, *Clinic. Pharmac. Biotechnology*, 2023, **24**(1), 61–85.
99 X. Huang, X. Qi, F. Boey and H. Zhang, *Chem. Soc. Rev.*, 2012, **41**, 666–686.
100 D. Chen, L. Tang and J. Li, *Chem. Soc. Rev.*, 2010, **39**, 3157–3180.
101 S. Pei, Q. Wei and K. Huang, *Nat. Commun.*, 2018, **9**, 145.
102 M. S. Umekar, R. G. Chaudhary, G. S. Bhusari, A. Mondal, A. K. Potbhare and M. Sami, *Mater. Today: Proc.*, 2020, **29**, 709–714.
103 R. Upadhyay, N. Soinb and S. Roy, *RSC Adv.*, 2014, **4**, 3823.
104 A. Fujishima and K. Honda, *Nature*, 1972, **238**, 37–38.
105 M. Abd Elkodous, G. S. El-Sayyad, M. A. Maksoud, R. Kumar, K. Maegawa, G. Kawamura and A. Matsuda, *J. Hazard. Mater.*, 2021, **410**, 124657.
106 F. Zhang, X. Wang, H. Liu, C. Liu, Y. Wan and Y. Long, *Appl. Sci.*, 2019, **9**(12), 2489.
107 R. Kumar, S. Sahoo, E. Joanni, R. K. Singh and K. K. Kar, *ACS Appl. Mater. Interfaces*, 2021, **14**(18), 20306–20325.
108 R. Kumar, S. Sahoo, E. Joanni, R. Pandey and J. J. Shim, *Chem. Commun.*, 2023, **59**(41), 6109–6127.
109 R. Kumar, S. Sahoo, E. Joanni and R. K. Singh, *J. Energy Chem.*, 2022, **74**, 252–282.
110 R. Kumar, S. Sahoo, E. Joanni, R. Pandey, W. K. Tan, G. Kawamura and A. Matsuda, *J. Energy Storage*, 2023, **68**, 107820.
111 S. M. Youssry, M. Abd Elkodous, R. Kumar, G. Kawamura, W. K. Tan and A. Matsuda, *Electrochim. Acta*, 2023, **463**, 142814.
112 R. Kumar, S. M. Youssry, E. Joanni, S. Sahoo, G. Kawamura and A. Matsuda, *J. Energy Storage*, 2022, **56**, 105896.
113 R. Kumar, R. K. Singh, P. K. Dubey, D. P. Singh, R. M. Yadav and R. S. Tiwari, *RSC Adv.*, 2015, **5**(10), 7112–7120.
114 S. M. Youssry, I. S. El-Hallag, R. Kumar, G. Kawamura, W. K. Tan, A. Matsuda and M. N. El-Nahass, *J. Energy Storage*, 2022, **50**, 104638.
115 R. Kumar, R. K. Singh, A. R. Vaz and S. A. Moshkalev, *RSC Adv.*, 2015, **5**(83), 67988–67995.
116 H. Su and Y. H. Hu, *Sci. Eng.*, 2020, **1**, 1–26.
117 R. Arukula, M. Vinothkannan, A. Kim and D. Yoo, *J. Alloys Compd.*, 2019, **771**, 477–488.
118 C. Botas, P. Alvarez, P. Blanco and R. Menéndez, *Carbon*, 2013, **65**, 156–164.
119 P. Boehm, R. Setton and E. Stumpp, *Carbon*, 1986, **24**, 241.
120 G. Long, C. Tang, K. Wong, C. Man, M. Fan, W. Lau, T. Xuc and B. Wang, *Green Chem.*, 2013, **15**, 821–828.
121 K. K. H. De Silva, H. Huang, R. K. Joshi and M. Yoshimura, *Carbon*, 2017, **119**, 190–199.
122 Y. Wang, Z. Shi and J. Yin, *ACS Appl. Mater. Interfaces*, 2011, **3**, 1127–1133.
123 P. B. Chouke, A. K. Potbhare, K. M. Dadure, A. J. Mungole, N. P. Meshram, R. R. Chaudhary, A. R. Rai and R. G. Chaudhary, *Mater. Today: Proc.*, 2022, **29**, 815–821.
124 R. K. Upadhyay, N. Soinb and S. Roy, *RSC Adv.*, 2014, **4**, 3823–3851.
125 D. Wang, *ACS Nano*, 2003, **4**, 1587–1595.
126 M. Chakrabarti, C. Low, N. Brandon, V. Yufit, M. Hashim, M. Irfan, J. Akthar, E. Ruiz-Trejo and M. hussain, *Electrochim. Acta*, 2013, **107**, 425–440.
127 A. W. Anwar, *J. Mater. Sci. Technol.*, 2015, **31**, 699–707.
128 W. Zhang, F. Liu, Q. Li, Q. Shou and J. Cheng, *Phys. Chem. Chem. Phys.*, 2012, **14**, 16331–16337.
129 P. Singh, P. Shandilya, P. Raizada, A. Sudhaik, A. Rahmani-sani and A. Hosseini-bandegharaei, *Arabian J. Chem.*, 2020, **13**, 3498–3520.
130 H. Zhang, X. Lv, Y. Li, Y. Wang and J. Li, *ACS Nano*, 2010, **4**, 380–386.
131 Y. Wang, Y. Li, L. Tang, J. Lu and J. Li, *Electrochem. Commun.*, 2009, **11**, 889–892.
132 J. Chen, B. Yao, C. Li and G. Shi, *Carbon*, 2013, **64**, 225–229.
133 D. Dreyer, S. Park, C. Bielawski and R. Ruoff, *Chem. Soc. Rev.*, 2010, **39**, 228–240.
134 N. Sorokina, M. Khaskov, V. Avdeev and I. Nikol'Skaya, *Russ. J. Gen. Chem.*, 2005, **75**, 162–168.
135 D. C. Marcano, D. V. Kosynkin, J. M. Berlin, A. Sinitskii, Z. Sun, A. Slesarev, L. B. Alemany, W. Lu and J. M. Tour, *ACS Nano*, 2010, **4**(8), 4806–4814.
136 Y. Xu, K. Sheng, C. Li and G. Shi, *J. Mater. Chem.*, 2011, **21**, 7376–7380.
137 M. Ajorloo, M. Fasihi, M. Ohshima and K. Taki, *Mater. Des.*, 2019, **181**, 108068.
138 P. V. Kumar, N. M. Bardhan, S. Tongay, J. Wu, A. M. Belcher and J. C. Grossmann, *Nat. Chem.*, 2014, **6**, 151–158.
139 B. Wang, Q. Liu, J. Han, X. Zhang, J. Wang, Z. Li, H. Yan and L. Liu, *J. Mater. Chem. A*, 2014, **2**, 1137–1143.
140 M. Rajabi, K. Mahanpoor and O. Moradi, *Composites, Part B*, 2019, **167**, 544–555.
141 B. Feng, J. Xie, C. Dong, S. Zhang, G. Cao and X. Zhao, *RSC Adv.*, 2014, **4**, 17902–17907.
142 V. H. Pham, T. T. Dang, K. Singh, S. H. Hur, E. W. Shin, J. S. Kim, M. A. Lee, S. H. Baeck and J. S. Chung, *J. Mater. Chem. A*, 2013, **1**, 1070–1077.
143 A. N. Abbas, G. Liu, A. Narita, M. Orosco, X. Feng, K. Müllen and C. Zhou, *J. Am. Chem. Soc.*, 2014, **136**, 7555–7558.
144 I. K. Moon, J. Lee, R. S. Ruoff and H. Lee, *Nat. Commun.*, 2010, **1**, 73–78.
145 M. McAllister, J. Li, D. Adamson, H. Schniepp, A. Abdala, J. Liu, M. Herrera-Alonso, D. Milius, R. Car, R. Prud'homme and I. Aksay, *Chem. Mater.*, 2007, **19**, 4396–4404.
146 L. Song, F. Khoerunnisa, W. GaoGao, W. Dou and T. Hayashi, *Carbon*, 2013, **52**, 608–612.

147 B. Shen, D. Lu, W. Zhai and W. Zheng, *J. Mater. Chem. C*, 2013, **1**, 50–53.
148 T. Kuila, A. K. Mishra, P. Khanra, N. H. Kim and J. H. Lee, *Nanoscale*, 2013, **5**, 52–71.
149 J. Yang, M. R. Jo, M. Kang, Y. S. Huh, H. Jung and Y. M. Kang, *Carbon*, 2014, **53**, 106–113.
150 J. A. Gerbec, D. Magana, A. Washington and G. F. Strouse, *J. Am. Chem. Soc.*, 2005, **127**, 15791–15800.
151 H. Hu, X. Wang, F. Liu, J. Wang and C. Xu, *Syn. Met.*, 2011, **161**, 404–410.
152 B. Tryba, A. W. Morawski and M. Inagaki, *Carbon*, 2005, **43**, 2417–2419.
153 Z. Li, Y. Yao, Z. Lin, K. S. Moon, W. Lin and C. Wong, *Mater. Chem.*, 2010, **20**, 4781–4783.
154 G. Demazeau, *J. Mater. Chem.*, 1999, **9**, 15–18.
155 J. T. Robinson, X. Li and H. Dia, *J. Mater. Chem.*, 2009, **131**, 9910–9911.
156 Y. Zhou, Q. Bao, L. A. L. Tang, Y. Zhong and K. P. Loh, *Chem. Mater.*, 2009, **21**, 2950–2956.
157 R. Wang, Y. Wang, C. Xu, J. Sun and L. Gao, *RSC Adv.*, 2013, **3**, 1194–1200.
158 S. Dubin, S. Gilje, K. Wang, V. C. Tung, K. Cha and A. S. Hall, *RSC Adv.*, 2010, **4**, 3845–3852.
159 D. Zhou, Q.-Y. Cheng and B.-H. Han, *Carbon*, 2011, **49**, 3920–3927.
160 J. Xiao, W. Lv and Z. Xie, *J. Mater. Chem. A*, 2016, **4**, 12126–12135.
161 O. A. Rahman, V. Chellasamy, N. Ponpandian, S. Amirthapandian, B. Panigrahi and P. Thangadurai, *RSC Adv.*, 2014, **4**, 56910–156917.
162 M. Fernandez-Merino, L. Guardia, L. Paredes, S. Villar-Rodil, P. olis-Fernandez and A. Martinez-Alonso, *J. Phys. Chem. C*, 2010, **114**, 6426–6432.
163 C. Bosch-Navarro, E. Coronado, C. Martí-Gastaldo, J. Sánchez-Royo and M. G. Gómez, *Nano*, 2012, **4**, 3977–3982.
164 Z. Bo, X. Shuai, S. Mao, H. Yang, J. Qian and J. Chen, *Sci. Rep.*, 2014, **4**(1), 4684.
165 S. Liu, J. Tian, L. Wang and X. Sun, *Carbon*, 2011, **49**, 3158–3164.
166 D. Wan, C. Yang, T. Lin, Y. Tang, M. Zhou and Y. Zhong, *ACS Nano*, 2012, **6**(1), 9068–9078.
167 C. Chua, A. Ambrosi and M. Pumera, *J. Mater. Chem. A*, 2012, **22**, 11054–11061.
168 J. Xiao, W. Lv and Z. Xie, *J. Mater. Chem. A*, 2016, **4**, 12126–12135.
169 A. Esfandiar, O. Akhavan and A. Irajizad, *J. Mater. Chem.*, 2011, **21**, 10907–10914.
170 X. Fan, W. Peng, Y. Li, X. Li, S. Wang and G. Zhang, *Adv. Mater.*, 2008, **20**, 4490–4493.
171 X. Mei and J. Ouyang, *Carbon*, 2011, **49**, 5389–5397.
172 H. L. Guo, X. F. Wang and Q. Y. Qian, *ACS Nano*, 2009, **3**, 2653–2659.
173 M. Khan, A. Al-Marri, M. Khan, N. Mohri, S. Adil, A. Al-Warthan, M. Siddiqui, H. Alkhathlan, R. Berger and W. Tremel, *RSC Adv.*, 2014, **4**, 24119–24125.
174 E. Nagaraj, A. Al-Marri, S. Vignesh, M. Srinivasan, G. Venkatesh, G. Palanisamy, P. Ramasamy, B. Palanivel, M. Al-Enizi, M. Ubaidullah, V. Reddy and W. Kim, *J. Alloys. Compd.*, 2022, **906**, 164255.
175 J. Li, G. Xiao, C. Chen and R. Li, *J. Mater. Chem. A*, 2013, **1**, 1481–1487.
176 T. Kuila, S. Bose, P. Khanra, A. K. Mishra, N. H. Kim and J. H. Lee, *Carbon*, 2012, **50**, 914–921.
177 G. Wang, F. Qian, C. Saltikov, Y. Jiao and Y. Li, *Nano Res.*, 2011, **4**, 563–570.
178 A. K. Potbhare, M. S. Umekar, P. B. Chouke, M. B. Bagade, S. K. Tarik Aziz, A. A. Abdala and R. G. Chaudhary, *Mater. Today: Proc.*, 2020, **29**, 720–725.
179 B. Feng, J. Xie, C. Dong, S. Zhang, G. Cao and X. Zhao, *RSC Adv.*, 2014, **4**, 17902–17907.
180 P. Khanra, T. Kuila, N. H. Kim, S. H. Bae, D.-S. Yu and J. H. Lee, *Chem. Eng. J.*, 2012, **183**, 526–533.
181 Z. Bo, X. Shuai, S. Mao, H. Yang, J. Qian, J. Chen, J. Yan and K. Cen, *Sci. Rep.*, 2014, **4**, 4684.
182 H.-J. Chu, C.-Y. Lee and N.-H. Tai, *Carbon*, 2014, **80**, 725–733.
183 S. K. Srivastava, C. Ogino and A. Kondo, *RSC Adv.*, 2014, **4**, 5986–5989.
184 M. J. Firdhouse and P. Lalitha, *Int. Nano Lett.*, 2014, **4**, 103–108.
185 D. Suresh, P. Nethravathi, H. Nagabhushana and S. Sharma, *Ceram. Int.*, 2015, **41**, 4810–4813.
186 S. B. Maddinedi, B. K. Mandal, R. Vankayala, P. Kalluru and S. R. Pamanji, *Spectrochim. Acta, Part A*, 2015, **145**, 117–124.
187 R. K. Upadhyay, N. Soin, G. Bhattacharya, S. Saha, A. Barman and S. S. Roy, *Mater. Lett.*, 2015, **160**, 355–358.
188 M. Khan, A. H. Al-Marri, M. Khan, M. R. Shaik, N. Mohri, S. F. Adil, M. Kuniyil, H. Z. Alkhathlan, A. Al-Warthan and W. Tremel, *Nanoscale Res. Lett.*, 2015, **10**, 281.
189 F. Tavakoli, M. Salavati-Niasari and F. Mohandes, *Mater. Res. Bull.*, 2015, **63**, 51–57.
190 T. Vu, T. Tran, H. Le, P. Nguyen, N. Bui and N. Essayem, *Mater. Sci.*, 2015, **38**, 667–671.
191 W. Han, W.-Y. Niu, B. Sun, G.-C. Shi and X.-Q. Cui, *J. Photochem. Photobiol., B*, 2016, **165**, 305–309.
192 D. Hou, Q. Liu, H. Cheng, K. Li, D. Wang and H. Zhang, *Mater. Chem. Phys.*, 2016, **183**, 76–82.
193 P. Chamoli, R. Sharma, M. K. Das and K. K. Kar, *RSC Adv.*, 2016, **6**, 96355–96366.
194 X. Jiang, Z. Li, J. Yao, Z. Shao and X. Chen, *Mater. Sci. Eng., C*, 2016, **68**, 798–804.
195 S. Sadhukhan, T. Ghosh, D. Rana, I. Roy, A. Bhattacharyya, G. Sarkar, M. Chakraborty and D. Chattopadhyay, *Mater. Res. Bull.*, 2016, **79**, 41–51.
196 C. Li, Z. Zhuang, X. Jin and Z. Chen, *Appl. Surf. Sci.*, 2017, **422**, 469–474.
197 X. Weng, J. Wu, L. Ma, G. Owens and Z. Chen, *Chem. Eng. J.*, 2019, **359**, 976–981.
198 R. Zaid, F. Chong, E. Teo, E. Ng and K. Chong, *Arabian J. Chem.*, 2015, **8**, 560–569.
199 D. Suresh, M. P. Kumar, H. Nagabhushana and S. Sharma, *Mater. Lett.*, 2015, **151**, 93–95.

200 B. Kartick and S. Srivastava, *J. Nanosci. Nanotechnol.*, 2013, **13**, 4320–4324.
201 S. Hatamie, O. Akhavan, S. K. Sadrnezhaad, M. M. Ahadian, M. M. Shirolkar and H. Q. Wang, *Mater. Sci. Eng., C*, 2015, **55**, 482–489.
202 R. Liao, Z. Tang, Y. Lei and B. Guo, *J. Phys. Chem. C*, 2011, **115**, 20740–20746.
203 O. Akhavan, M. Kalaee, Z. Alavi, S. Ghiasi and A. Esfandiar, *Carbon*, 2012, **50**, 3015–3025.
204 B. Haghighi and M. A. Tabrizi, *RSC Adv.*, 2013, **3**, 13365–13371.
205 A. Singh, B. Ahmed, A. Singh and A. K. Ojha, *Spectrochim. Acta, Part A*, 2018, **204**, 603–610.
206 S. Shahane and D. Sidhaye, *Int. J. Mod. Phys. B*, 2018, **32**, 1840068.
207 J. R. Anasdass, P. Kannaiyan, R. Raghavachary, S. C. Gopinath and Y. Chen, *PLoS One*, 2018, **13**, e0193281.
208 W. Ye, X. Li, J. Luo, X. Wang and R. Sun, *Ind. Crops Prod.*, 2017, **109**, 410–419.
209 B. Chandu, V. Mosali, B. Mullamuri and H. Bollikolla, *Carbon Lett.*, 2017, **21**, 74–80.
210 D. Hou, Q. Liu, H. Cheng and K. Li, *J. Nanosci. Nanotechnol.*, 2017, **17**, 6518–6523.
211 F.-Y. Xing, L.-L. Guan, Y.-L. Li and C.-J. Jia, *Environ. Toxicol. Pharmacol.*, 2016, **48**, 110–115.
212 G. Lee and B. S. Kim, *Biotechnol. Prog.*, 2014, **30**, 463–469.
213 S. Gurunathan, J. W. Han, J. H. Park, V. Eppakayala and J. H. Kim, *Int. J. Nanomed.*, 2014, **9**, 363–377.
214 B. Haghighi and M. A. Tabrizi, *RSC Adv.*, 2013, **3**, 13365–13371.
215 C. Zhu, S. Guo, Y. Fang and S. Dong, *ACS Nano*, 2010, **4**, 2429–2437.
216 N. H. Kim, P. Khanra, T. Kuila, D. Jung and J. H. Lee, *J. Mater. Chem. A*, 2013, **1**, 11320–11328.
217 B. Haghighi and M. A. Tabrizi, *RSC Adv.*, 2013, **3**, 13365–13371.
218 J. Zhang, H. Yang, G. Shen, P. Cheng, J. Zhang and S. Guo, *Chem. Comm.*, 2010, **46**, 1112–1114.
219 D. Chen, L. Li and L. Guo, *Nanotech*, 2011, **22**, 325601.
220 Y. Wang, Z. Shi and J. Yin, *ACS Appl. Mater. Interfaces*, 2011, **3**, 1127–1133.
221 K. Loh, Q. Bao, K. Ang and J. Yang, *J. Mater. Chem.*, 2012, **20**, 2277–2289.
222 H. Bai, C. Li and G. Shi, *Adv. Mater.*, 2011, **23**, 1089–1115.
223 S. Yang, W. Yue, D. Huang, C. Chen, H. Lin and X. Yang, *RSC Adv.*, 2012, **2**, 8827–8832.
224 H. Su and H. Hu, *Energy Sci. Eng.*, 2021, **9**, 958–983.
225 J. Bai, D. Liu, J. Yang and Y. Chen, *ChemSusChem*, 2019, **12**, 2117–2132.
226 M. Iqbal, A. Rehman and S. Siddique, *J. Energy Chem.*, 2019, **39**, 217–234.
227 N. Elavarasan, S. Prakasha, K. Kokilaa, C. Thirunavukkarasuc and V. Sujatha, *New J. Chem.*, 2020, **44**, 2166–2179.
228 F. Meng, H. Zheng, Y. Chang, Y. Zhao, M. Li and C. Wang, *IEEE Trans. Nanotechnol.*, 2018, **17**, 212–219.
229 H. Al-Marri, M. Khan, M. Shaik, N. Mohri, S. Adil, M. Kuniyil, H. Alkhathlan, A. Al-Warthan, W. Tremel, M. Tahir, M. Khan, M. Rafiq and H. Siddiqui, *Arabian J. Chem.*, 2016, **9**, 835–845.
230 X. Zhang, *J. Mater. Chem.*, 2010, **20**, 2801–2806.
231 C. Hintze, *J. Eur. Ceram. Soc.*, 2016, **36**, 2923–2930.
232 S. Nayak, A. Soam, J. Nanda, C. Mahender, M. Singh, D. Mohpatra and R. Kumar, *J. Mater. Sci.: Mater. Electron.*, 2018, **29**, 9361–9368.
233 W. Li, F. Wang, S. Feng, J. Wang, Z. Sun, B. Li, Y. Li, J. Yang, A. Elzatahry, Y. Xia and D. Zhao, *J. Am. Chem. Soc.*, 2013, **135**, 18300–18303.
234 R. K. Singh, R. Kumar, D. P. Singh, R. Savu and S. A. Moshkalev, *Mater. Today Chem.*, 2019, **12**, 282–314.
235 H. Hassan, V. Abdelsayed, R. Khder, K. AbouZeid, J. Terner, M. ElShall, S. Al-Resayes and A. El-Azhary, *J. Mater. Chem.*, 2009, **19**, 3832–3837.
236 A. Dey, S. Panja, A. K. Sikder and S. Chattopadhyay, *RSC Adv.*, 2015, **5**(14), 10358–10364.
237 R. Kumar, S. M. Youssry, M. M. Abdel-Galeil and A. Matsuda, *J. Mater. Sci.: Mater. Electron.*, 2020, **31**, 15456–15465.
238 S. Chabi, C. Peng, Z. Yang, Y. Xia and Y. Zhu, *RSC Adv.*, 2015, **5**, 3999–4008.
239 J. Shen, M. Shi, H. Ma, B. Yan, N. Li and M. Ye, *Mater. Res. Bull.*, 2011, **46**, 2077–2083.
240 D. K. Padhi, T. Panigrahi, K. Parida, S. K. Singh and P. M. Mishra, *ACS Sustainable Chem. Eng.*, 2017, **5**, 10551–10562.
241 R. G. Chaudhary, A. K Potbhare, S. K. Tarik Aziz, M. S. Umekar, S. S. Bhuyar and A. Mondal, *Mater. Today: Proc.*, 2021, **36**, 756–762.
242 P. Kumbhakar, A. Pramanik, S. Biswas, A. K. Kole, R. Sarkar and P. Kumbhakar, *J. Hazard. Mater.*, 2018, **360**, 193–203.
243 M. Hamid, M. Rianna, W. R. Rangkuti, T. Sembiring and P. Sebayang, *S. Afr. J. Chem. Eng.*, 2022, **42**, 280–282.
244 X. Yang, C. Chen, J. Li, G. Zhao, X. Ren and X. Wang, *RSC Adv.*, 2012, **2**, 8821–8826.
245 G. Cai, J. Tu, J. Zhang, Y. Mai, Y. Lu, C. Guab and X. Wang, *Nanoscale*, 2012, **4**, 5724–5730.
246 W. Qian, Z. Chen, S. Cottingham, W. Alexander, A. Natasja, A. M. Goforth, T. L. Clarec and J. Jiao, *Green Chem.*, 2012, **14**, 371–377.
247 G. Jeevitha, R. Abhinayaa, D. Mangalaraj, N. Ponpandian, P. Meena, V. Mounasamy and S. Madanagurusamy, *Nanoscale Adv.*, 2019, **1**, 1799–1811.
248 K. Rahimi, H. Zafarkish and A. Yazdani, *Mater. Des.*, 2018, **144**, 214–221.
249 R. Elshypany, H. Selim, K. Zakaria, A. H. Moustafa, S. A. Sadeek, S. I. Sharaa, P. Raynaud and A. A. Nada, *Molecules*, 2021, **14**, 2269.
250 S. Hamed, K. Hossain, S. Masoud, S. Niasari and D. Mortazavi, *J. Colloid Interface Sci.*, 2017, **498**, 423–432.
251 H. Zhang, X. Lv, Y. Li, Y. Wang and J. Li, *ACS Nano*, 2010, **4**, 380–386.
252 S. Chandra, P. Das, S. B. P. Pramanik and P. Pramanik, *Mater. Sci. Eng., B*, 2012, **177**, 855–861.

253 B. N. Benjwal, M. Kumar, P. Chamoli and K. K. Kar, *RSC Adv.*, 2015, **5**, 73249–73260.
254 Y. Fu and X. Wang, *Ind. Eng. Chem. Res.*, 2011, **50**, 7210–7218.
255 T. Lv, L. Pan, X. Liu, T. Lu, G. Zhu and Z. Sun, *J. Alloys Compd.*, 2011, **509**, 10086–10091.
256 S. Thangavel, G. Venugopal and K. Jae, *Mater. Chem. Phys.*, 2014, **145**, 108–115.
257 K. Sharma, K. Maiti, N. H. Kim, D. Hui and J. H. Lee, *Composites, Part B*, 2018, **138**, 35–44.
258 A. Isari, A. Payan, M. Fattahi, S. Jorfi and B. Kakavandi, *Appl. Surf. Sci.*, 2018, **462**, 549–564.
259 R. G. Chaudhary, V. Sonkusare, G. Bhusari, A. Mondal, A. Potbhare, H. Juneja and R. Sharma, *Environ. Res.*, 2023, **222**, 115363.
260 S. K. T. Aziz, M. Awasthi, S. Guria, M. Umekar, I. Karajagi, S. K. Riyajuddin, K. V. Siddhartha, A. Saini, A. Potbhare, R. G. Chaudhary and V. Vishal, *STAR Protoc.*, 2023, **4**(3), 102448.
261 Z. Song, Y.-L. Ma and C.-E. Li, *Sci. Total Environ.*, 2019, **651**, 580–590.
262 S. Shanavas, A. Priyadharsan, E. I. Gkanas, R. Acevedo and P. M. Anbarasan, *J. Ind. Eng. Chem.*, 2019, **72**, 512–528.
263 L. Lin, H. Wang and P. Xu, *Chem. Ind. Eng. J.*, 2017, **310**, 389–398.
264 L. Pastrana-Martínez, S. MoralesTorres, V. Likodimos, J. Figueiredo, J. Faria and P. Falaras, *Appl. Catal., B*, 2012, **123**, 241–256.
265 Z. Wan and J. Wang, *J. Hazard. Mater.*, 2017, **324**, 653–664.
266 R. Karthik, V. J. Kumar, S.-M. Chen, C. Karuppiah, Y.-H. Cheng and V. A. Muthuraj, *ACS Appl. Mater. Interfaces*, 2017, **9**, 6547–6559.
267 G. Malekshoar, K. Pal, Q. He, A. Yu and A. K. Ray, *Ind. Eng. Chem. Res.*, 2014, **53**, 18824–18832.
268 S. Jo W-K, S. Kumar, M. Isaacs, A. Lee and S. Karthikeyan, *Appl. Catal., B*, 2017, **201**, 159–168.
269 L. Ji, Z. Tan, T. R. Kuykendall, S. Aloni, S. Xun, E. Lin, V. Battaglia and Y. Zhang, *Phys. Chem. Chem. Phys.*, 2011, **13**, 7170.
270 A. Staffolani, H. Darjazi, G. Carbonari, F. Maroni, S. Gabrielli and F. Nobili, *Molecules*, 2016, **26**, 4316.
271 N. Kumar, J. R. Rodriguez, V. G. Pol and A. Sen, *Appl. Surf. Sci.*, 2019, **463**, 132–140.
272 B. Xiao, B. Zhang, L. B. Tang, C. S. An, Z. J. He, H. Tong, W. J. Yu and J. C. Zheng, *Ceram. Int.*, 2018, **44**(13), 15044–15049.
273 N. Naresh, D. Narsimulu, P. Jena, S. R. E. S. Dhu and N. Satyanarayana, *J. Mater. Sci.: Mater. Electron.*, 2018, **29**, 14723–14732.
274 S. T. Aziz, M. Ummekar, I. Karajagi, S. K. Riyajuddin, K. V. R. Siddhartha, A. Saini, A. Potbhare, R. G. Chaudhary, V. Vishal, P. C. Ghosh and A. Dutta, *Cell Rep. Phys. Sci.*, 2022, **3**, 101106.
275 R. B. Suneetha, P. Selvi and C. Vedhi, *Vacuum*, 2019, **164**, 396–404.
276 J. Jayachandiran, J. Yesuraj, M. Arivanandhan, A. Raja, S. A. Suthanthiraraj, R. Jayavel and D. Nedumaran, *J. Inorg. Organomet. Polym. Mater.*, 2018, **28**, 2046–2055.
277 W. H. Low, P. S. Khiew, S. S. Lim, C. W. Siong and E. R. Ezeigwe, *J. Alloys Compd.*, 2018, **768**, 995–1005.
278 C. K. Maity, G. Hatui, K. Verma, G. Udayabhanu, D. D. Pathak and G. C. Nayak, *Vacuum*, 2018, **157**, 145–154.
279 S. Nagarani, G. Sasikala, K. Satheesh, M. Yuvaraj and R. Jayavel, *J. Mater. Sci.: Mater. Electron.*, 2018, **29**, 11738–11748.
280 Z. Wu, S. Yang, Y. Sun, K. Parvez, X. Feng and K. Müllen, *J. Am. Chem. Soc.*, 2018, **134**, 9082–9085.
281 J. Xiao, Q. Kuang, S. Yang, F. Xiao, S. Wang and L. Guo, *Sci. Rep.*, 2013, **3**, 2300.
282 R. Arukula, M. Vinothkannana, A. Rhan, K. Dong and J. Yoo, *J. Alloys Compd.*, 2019, **771**, 477–488.
283 B. Baruah, A. Kumar, G. Umapathy and S. Ojha, *J. Electroanal. Chem.*, 2019, **840**, 35–51.
284 Y. C. Cao, C. Xu and X. Wu, *J. Power Sources*, 2011, **196**, 8377–8382.
285 N. A. Kotov, *Nature*, 2006, **442**, 254–255.
286 M. Zhang, L. Su and L. Mao, *Carbon*, 2006, **44**, 276–283.
287 D.-W. Wang, F. Li, M. Liu, G. Lu and H. Cheng, *Angew. Chem.*, 2008, **120**, 379–382.
288 J. Liu, J. Shen, M. Li and L. Guo, *Chin. Chem. Lett.*, 2015, **26**, 1478–1484.
289 M. Khan, M. Khan and M. Cho, *Nanoscale*, 2018, **10**, 9427–9440.
290 X. Li, J. Yu and M. Jaroniec, *Chem. Soc. Rev.*, 2016, **45**, 2603–2636.
291 X. Lü, J. Shen, J. Wang, Z. Cui and J. Xie, *RSC Adv.*, 2015, **5**, 15993–15999.
292 A. Ajmal, I. Majeed, R. N. Malik, H. Idriss and M. A. Nadeem, *RSC Adv.*, 2014, **4**, 37003–37026.
293 R. Molinari, C. Lavorato and P. Argurio, *Chem. Eng. J.*, 2015, **274**, 307–316.
294 S. K. Yadav, R. Kumar, A. K. Sundramoorthy, R. K. Singh and C. M. Koo, *RSC Adv.*, 2016, **6**(58), 52945–52949.
295 S. Vadahanambi, J. H. Jung, R. Kumar, H. J. Kim and I. K. Oh, *Carbon*, 2013, **53**, 391–398.
296 H. M. El-Bery, Y. Matsushita and A. Abdel-moneim, *Appl. Surf. Sci.*, 2017, **423**, 185–196.
297 T. T. Wei, P. Peng, Y. R. Ji, Y. R. Zhu, T. F. Yi and Y. Xie, *J. Energy Chem.*, 2022, **71**, 400–410.
298 T. F. Yi, L. Shi, X. Han, F. Wang, Y. Zhu and Y. Xie, *Energy Environ. Mater.*, 2021, **4**(4), 586–595.
299 H. Chang, Y. R. Wu, X. Han and T. F. Yi, *Energy Mater.*, 2021, **1**(3), 24.
300 B. Li and H. Cao, *J. Mater. Chem.*, 2011, **21**, 3346.
301 L. Sun, Y. Zhang and D. Zhang, *Nanoscale*, 2017, **9**, 18552–18560.
302 C. Lin, L. Hu and C. Cheng, *Electrochim. Acta*, 2018, **260**, 65–72.
303 L. Bai, Y. Zhang and L. Zhang, *Nano Energy*, 2018, **53**, 982–992.
304 B. Kirubasankar, B. Murugadoss and V. Lin, *Nanoscale*, 2018, **10**, 20414–20425.

305 T. F. Yi, H. M. K. Sari, X. Li, F. Wang, Y. R. Zhu, J. Hu and X. Li, *Nano Energy*, 2021, **85**, 105955.
306 T. F. Yi, L. Y. Qiu, J. Mei, S. Y. Qi, P. Cui, S. Luo and Y. B. He, *Sci. Bull.*, 2020, **65**, 546–556.
307 J. Han, L. L. Zhang and S. Lee, *ACS Nano*, 2013, **7**, 19–26.
308 S. Xiong, B. Yang, D. Cai, G. Qiu and Z. Wu, *Electrochim. Acta*, 2015, **185**, 52–61.
309 J. Zhang, C. Guo, L. Zhang and C. Li, *Chem. Commun.*, 2013, **49**, 6334–6336.
310 A. Marinoiu, M. Raceanu, E. Carcadea and M. Varlam, *Appl. Surf. Sci.*, 2018, **456**, 238–245.